JAERI-Data/Code
2000-042

MEASUREMENT OF ACTIVATION REACTION RATE DISTRIBUTION ON A MERCURY TARGET WITH A LEAD-REFLECTOR AND LIGHT-WATER-MODERATOR FOR HIGH ENERGY PROTON BOMBARDMENT USING AGS ACCELERATOR

February 2001

Yoshimi KASUGAI, Hiroshi TAKADA, Shin-ichiro MEIGO,
Fujio MAEKAWA, Hiroshi NAKASHIMA, Yujiro IKEDA,
Takashi INO*, Setuo SATO*, Eric JERDE* and David GLASGOW*

日本原子力研究所
Japan Atomic Energy Research Institute

本レポートは，日本原子力研究所が不定期に公刊している研究報告書です。
入手の問合わせは，日本原子力研究所研究情報部研究情報課（〒319-1195　茨城県那珂郡東海村）あて，お申し越しください。なお，このほかに財団法人原子力弘済会資料センター（〒319-1195　茨城県那珂郡東海村日本原子力研究所内）で複写による実費頒布をおこなっております。

This report is issued irregularly.
Inquiries about availability of the reports should be addressed to Research Information Division, Department of Intellectual Resources, Japan Atomic Energy Research Institute, Tokai-mura, Naka-gun, Ibaraki-ken, 319-1195, Japan.

編集兼発行　　日本原子力研究所

JAERI-Data/Code 2000-042

Measurement of Activation Reaction Rate Distribution on a Mercury Target with a Lead-reflector and Light-water-moderator for High Energy Proton Bombardment using AGS Accelerator

Yoshimi Kasugai, Hiroshi Takada, Shin-ichiro Meigo, Fujio Maekawa, Hiroshi Nakashima, Yujiro Ikeda, Takashi Ino[*1], Setuo Sato[*1], Eric Jerde[*2] and David Glasgow[*2]

Center for Neutron Science

Tokai Research Establishment

Japan Atomic Energy Research Institute

Tokai-mura, Naka-gun, Ibaraki-ken

(Received November 17, 2000)

Characteristic of spallation neutrons driven by GeV protons from a mercury target with a lead-reflector and light-water-moderator was studied experimentally using the Alternating Gradient Synchrotron (AGS) facility of Brookhaven National Laboratory in a framework of the ASTE (AGS Spallation Target Experiment) collaboration. Several reaction rates along with the mercury target were measured with the activation method at incident proton energies of 1.94, 12 and 24 GeV. Indium, niobium, aluminum, cobalt, nickel and bismuth were used as activation detectors to cover the threshold energy of between 0.33 and 40.9 MeV. This report summarizes the experimental procedure with all the measured data.

Keywords: ASTE Collaboration, AGS, Mercury, Lead-Reflector, Light-water-moderator, Spallation Target, Reaction Rate, 1.94, 12 and 24 GeV, Activation Detector

*1 High Energy Accelerator Research Institute

*2 Oak Ridge National Laboratory

JAERI-Data/Code 2000-042

ＡＧＳ加速器を使った高エネルギー陽子入射による鉛反射体及び軽水減速材付き水銀ターゲットの放射化反応率分布測定

日本原子力研究所東海研究所中性子科学研究センター
春日井　好己・高田　弘・明午　伸一郎・前川　藤夫・中島　宏・池田　裕二郎・猪野　隆[*1]・
佐藤　節夫[*1]・Eric Jerde [*2]・David Glasgow [*2]

（2000年11月17日受理）

ASTE (AGS Spallation Target Experiment)共同実験の一環として、ブルックヘブン国立研究所のAGS 加速器を使って、鉛反射体及び軽水減速材付き水銀ターゲットから GeV 領域の陽子入射によって発生する核破砕中性子の特性を実験的に調べた。入射陽子のエネルギー1.94、12及び24 GeVについて、水銀ターゲットに沿った位置における種々の反応率を放射化法で測定した。放射化検出器としては、インジウム、ニオブ、アルミニウム、コバルト、ニッケル及びビスマスを用い、0.33 から 40.9 MeV のしきいエネルギーをカバーした。本レポートは、実験方法及びすべての実験結果をまとめたものである。

東海研究所：〒319-1195　茨城県那珂郡東海村白方白根 2-4
[*1] 高エネルギー加速器研究機構
[*2] オークリッジ国立研究所

Contents

目次

1. Introduction

Intense neutron sources driven by GeV protons with power of MW are planning to be constructed for expanding fundamental researches in life science, material science, and so on. Neutrons are produced in a spallation process by bombarding a heavy-metal target with energetic protons from a high power accelerator. Mercury has been selected as a material of spallation neutron targets. [1, 2] Due to lack of the experimental data, however, the feasibility of the mercury target as the intense-neutron source has not been thoroughly examined yet. The experimental study of the fundamental characterization of mercury target is still strongly required to reach a precise design of the system. As a reflector and a moderator play important role in a spallation target assembly, optimization of those configurations is necessary to confirm the highest neutron performance for extraction of neutrons with respect to brightness and sharp time structure. A calculation code system for simulating nuclear interaction and particle transportation [3] is extensively being used for the optimization. To verify the code system, the mockup test of the target assembly has been required.

To satisfy those demands, an experiment using a mercury target has been proposed and carried out using Alternating Gradient Synchrotron (AGS) at Brookhaven National Laboratory in the framework of an international collaboration, whose name in ASTE (AGS Spallation Target Experiment). The ASTE collaboration was aimed at studying neutronics characteristic of the mercury target and mechanical properties of the target and its container in terms of pressure wave and induced stress associated with intense proton incident pulsed. The first and second experiments were carried out using a mercury target without any assembly around it on May 1997 and November 1998, respectively. The results of the experiments were reported in Refs. 4-10.

As the second step, the neutronics experiment for the mercury target with a lead-reflector and a light-water moderator was done on March 1999. In the experiment, reaction rate distributions, a thermal neutron spectrum, and heat deposition in the light-water moderator were measured using 1.94-, 12- and 24-GeV protons. This report deals with the measurement of the reaction rate. The experimental procedure is described in Section 2, and measured data are presented in Section 3. A discussion is also given by comparing the present reaction rate data to the previous data for the bare target.

2. Experiment

2.1 Mercury Target and Reflector Setup

A schematic plain view of the accelerator complex of Brookhaven National Laboratory is shown in Fig. 1. The mercury target was set in the U-line tunnel branched at the point between AGS and Relativistic Heavy Ion Collider (RHIC).

Mercury was contained in a cylindrical target container made of stainless steel with 2.5 mm in thickness. The dimension of the target container was 200 mm in inner diameter and 1300 mm in inner length. The upper and side views of the mercury target are shown in Fig. 2. The target container had a hemisphere beam incident surface on its top end, and had several flanges to install some instruments. The target container was put in the secondary container made from stainless steel with 3.5 mm in thickness. More detailed description of the target dimension is described in Ref. 4.

The secondary container was fixed on a movable platform and installed in a lead-reflector. Plain, front and cross sectional views of the target, reflector and moderator were shown in Fig. 3. There is an opening in a side of the lead reflector to extract neutrons for the TOF-measurement. The moderator which contained light-water was put in the lead-reflector. Through the opening the moderator can be seen. A plain and cross sectional view of the moderator box is shown in Fig.4. The relative position at the mercury target with the reflector and the moderator can be changed by moving the platform. The distance between the top of the mercury target and the center of the moderator was fixed on 200 mm for irradiation of the activation measurement.

The cross sectional view of the setup in U-line block house is shown in Fig. 5. The nominal height of the beam axis was 1250 mm from the ground. The center of the mercury target was placed at the beam axis. The moderated neutron beams were extracted from the opening in the lead reflector at the height of 1150 mm. For the TOF-measurement, a neutron collimator made of iron block was placed in front of a penetration, whose axis is corresponding to the opening.

2.2 Activation Detector Arrangement

The following high purity metal foils were employed as activation detectors: indium, aluminum, cobalt, nickel and bismuth. The size and purity of each foil is listed in Table 1. The decay properties of radionuclide which are the products of the reactions used for activation detectors are listed in Table 2. The threshold energies of the detectors range from 0.34 (^{115}In(n,n')^{115m}In) to 45 MeV (^{209}Bi(n,7n)^{203}Bi). The ^{115}In(n,n')^{115m}In reaction with the threshold energy of 0.3 MeV was mainly used for measurement of the

spatial distribution of the neutron flux.

Arrangement of an activation-detector-holder made of aluminum is shown in the left part of Fig. 6. Four holders were set on the side surface of the mercury target cylinder as shown in the left of Fig. 6. The activation detectors were mounted on the acrylic bars whose size was 22 mm in width, 9 mm in thickness and 1200 mm in length, and each bars was inserted into the holder fixed on the target container. Configuration of the holder, the acrylic bar and an activation-detector are shown in the right of Fig. 6. The four bars were indexed as "Main", "Sub-1", "Sub-2" and "Sub-3", respectively, as shown in the left of Fig. 6. The detectors on the Sub-1 and Sub-2 and Sub-3 bars were served to monitor the effect of the deviation of the beam incident point from the central axis of the mercury target.

The details of foil positions are shown in Fig. 7. Full set of the foils was set on the Main bar. On the Sub bars, the indium and niobium foils were set. Aluminum, cobalt, nickel and bismuth were assembled to one foil stack. The total thickness of the foil-stack was about 6 mm including the tape used for stacking the foils. The stacks were so thick that the effect of the position difference and neutron absorption was not negligible. Thus, indium foils were attached on each side of the stack to check the effects.

2.3 Irradiation

Experiments used proton beams with the different incident energies of 24, 12 and 1.94 GeV. The number of proton (N_p) was measured with an integrating current transformer (ICT), a separated-electron-chamber (SEC) and the activation method using the $Cu(p,x)^{24}Na$ reaction. The cross section of the $Cu(p,x)^{24}Na$ reaction has been studied relatively well for a wide proton energy range as shown in Fig 8, although there is some data scattered in the energy range from 1 GeV to 6 GeV. The N_p values of ICT were consistent with the activation method within 3%. This agreement was good enough considering the uncertainty of ± 8~10% associated with the activation method; the uncertainty was mainly due to the cross section uncertainty of the $Cu(n,x)^{24}Na$ reaction. The N_p values measured with SEC are also consistent with the values of ICT in 7%. In this work, the values of ICT were adopted to deduce reaction rates per incident proton. Determined N_p values were 7.0×10^{13}, 4.5×10^{13} and 2.0×10^{13} for the incident proton energies of 1.94, 12 and 24 GeV, respectively. The conditions of proton incidents of each irradiation were summarized in Table 3.

Proton beam profiles were measured with a strip ionization multi-wire chamber and an imaging-plate (IP). [11] The IP-images for 24 and 12 GeV proton bombardment are shown in Fig. 9. It was observed that the center of the beam profile was shifted in a few millimeters for each irradiation. For 1.94 GeV proton bombardment, the center of beam profile, however, was not observed clearly in the IP

image. The proton beam of 1.94 GeV was not focused well because AGS has not been optimized for acceleration of such low-energy protons.

2.4 Gamma-ray measurement of the activation detectors

After irradiation, the four acrylic bars supporting activation detectors were removed from the target and they were carried to a shed, and then the foils were dismounted. After foils were sorted and sealed in plastic bags one by one, they were transported to a counting room in the chemistry department building of Brookhaven National Laboratory. Gamma-rays from activated foils were measured with four germanium-detectors.

A series of measurements for short-lived radioactive products with half-lives less than 1 day was done in 12 hours after each irradiation. Second measurement for long-lived radionuclide (1~10 d) was done for a few days after the irradiation. Further measurement for long-lived radioactive products (>10 d) was carried out at Oak Ridge National Laboratory after transmitting the foils there.

2.5 Reaction Rate Deduction

The reaction rate of a produced nuclide is obtained using the following relation,

$$Y = \frac{\lambda \cdot C}{N_A \cdot \frac{w}{M} \cdot N_P \cdot a \cdot \varepsilon \cdot b \cdot \left(1 - e^{-\lambda T_r}\right) \cdot e^{-\lambda T_c} \cdot \left(1 - e^{-\lambda \cdot T_m}\right)} \tag{2.1}$$

where Y is reaction rate (/s), N_A is Avogadoro's number (/mol), w is weight of foil (g), M is atomic mass of target element (g/mol), N_p is number of incident protons (/s), λ is decay constant (/s), C is gamma-ray peak counts, ε is detection efficiency, a is natural abundance of target nucleus, b is branching ratio, T_r is irradiation time (s), T_c is cooling time (s) and T_m is measuring time (s).

The natural abundance of ^{93}Nb, ^{27}Al, ^{59}Co and ^{209}Bi is 100%, and that of ^{115}In is 97.5%. Since nickel contains five isotopes, the radionuclei of ^{58}Co and ^{57}Co can be produced via many different pathways from five isotopes. Thus, the a value for nickel is supposed to be 100% to deduce the reaction rate per target nucleus for all isotopes. The decay constants and the gamma-ray branching ratios were taken from Ref. 12; those data are listed in Table 2. The detection efficiency for each gamma-ray peaks was deduced by considering the size of the activation detectors, gamma-ray attenuation in the activation detectors and the cascade coincidence summing effect.

2.6 Error Estimation

The sources of experimental error were mainly attributed to the following items:

1) Statistical error of a gamma-ray peak count,

2) Error of a foil weight,

3) Error of the number of incident protons,

4) Error of the gamma ray detector efficiency

5) Error of a half-life and a gamma-ray emission rate.

The error of each item was listed in Table 4. The detector efficiency error was estimated to be ± 3~4% by considering the errors of activities of the standard sources for the calibration. The error of the number of protons measured by ICT was estimated to be ± 3% by considering the deviations among the three kinds of methods: ICT, SEC and the activation method.

The errors of the gamma-ray detector efficiency, the number of incident protons, the half-life and gamma-ray emission rate are intrinsic to the gamma-ray measurement. They are regarded as the systematic error, and denoted as δ_{sys}. The errors of foil weight are also regarded as systematic error. On the other hand, the error of the gamma-ray peak count is dependent upon individual measurement of foil. It is regarded as the statistical component of the error denoted as δ_{sta}. The total error δ_{tot} was deduced as

$$\delta_{tot} = \sqrt{\delta_{sta}^{\ 2} + \delta_{sys}^{\ 2}}\ .$$

In the next section, results of reaction rates are tabulated in tables with the statistical and total errors.

3. Result and Discussion

Measured reaction rates are given in tables. The format of the table is explained in Table 5. The reaction rates are plotted in Figs. 10 as a function of the distance from the top of the spherical surface of the mercury target to the foil position. The reaction rates of ^{115}In(n,n')^{115m}In are plotted in Fig. 10.1.1, 10.1.2 and 10.1.3 for 1.94, 12 and 24 GeV, respectively. As mentioned in Sec.2, the indium foils were set on all the bars: "Main", "Sub-1", "Sub-2" and "Sub-3". To see the difference of the reaction rates among the four bars clearly, the reaction rates were plotted in a linear-scale. For other reactions, the vertical axes of the figures are in a log-scale. To make the distribution clear, the reaction rate data were fitted with following equation:

$$Y = a_1 \exp(-a_2 x) + a_3 \exp(-a_4 x) + a_5 \exp(-a_6 x), \tag{3.1}$$

where Y is the reaction rate, x is the distance between the top of the mercury target and the detector position, and a_i (i=1, 2, ..., 6) are the fitting parameters. The fitting curves are shown in the figures, and the fitting parameters are tabulated in the Table 6.

As mentioned in the previous section, indium and niobium foils were set on all the bars to observe possible deviations of the reaction rates among the four bars. For the 24 GeV proton bombardment, the ^{115}In(n,n')^{115m}In reaction rates of Sub-2 and Sub-3 bars are larger than those of Main and Sub-1 bars by 30-40% as seen Fig. 10.1.3. The similar deviations can be seen for the ^{93}Nb(n,2n)^{92m}Nb and ^{93}Nb(n,4n)^{90}Nb reaction rates for 24 GeV in Figs. 10.2.3 and 10.3.3. These results imply that center of the proton beam distribution was shifted upward. However, the averaged proton beam profile slightly shifted to the down according to the beam profile measurement with IP as shown in Fig. 9. The deviation of the reaction rate is not consistent with the shift of the proton beam profile. The alignment of the beam profile monitor with the target assembly might not be accurate. According to the preliminary analysis using the NMTC/JAM-NCNP code [3], it is possible that the center of the beam profile monitor shifted upward by 2 cm. The deviations of the reaction rates on 12 GeV can also be explained well by the shift of the profile monitor.

The distribution of the reaction rate of the ^{115}In(n,n')^{115m}In reaction is effective to analyze the distribution of the total neutron flux from the mercury target since the threshold energy of the ^{115}In(n,n')^{115m}In reaction is low enough of 0.3 MeV. In Fig. 11.1, the averaged reaction rates of four bars are plotted as a function of the distance. The averaged reaction rates of the ^{93}Nb(n,2n)^{92m}Nb with the threshold energy of 9.06 MeV were also plotted for comparison in Fig. 11.2. In general, the peak position of the reaction rates moves to deeper position with increasing the incident proton energy for both reactions. The peak position of the reaction rate distribution for the ^{93}Nb(n,2n)^{92m}Nb reaction is nearer to the spherical surface than that for the ^{115}In(n,n')^{115m}In reaction. This means that the high-energy neutrons were

produced at the forward position of the mercury target. The distances of the peak positions for the ^{115}In(n,n')^{115m}In and ^{93}Nb(n,2n)^{92m}Nb reaction are plotted as the incident proton energy in Fig. 12.1 and 12.2, respectively. The data for the bare target experiment are also plotted for comparison. The data of peak positions are fitted with the equation of $x_p = a_1 + a_2 \log_{10} E_p$, where x_p is the peak position in cm, E_p is the incident neutron energy in GeV, and a_i (i=1, 2) is the fitting parameters. The fitting curve and parameters are shown in the figures. The fitting curves show the trend of the reaction rate distribution as a function of the incident proton energy. For the ^{115}In(n,n')^{115m}In reactions, as increasing the incident proton energy, the peak of the reaction rate distribution for the present target assembly moves to deeper position more rapidly than that for the bare. On the other hand, for the ^{93}Nb(n,2n)^{92m}Nb reaction, the variation trend of the curve for the present target assembly are almost same as that for the bare target.

In order to examine the effectiveness of the lead-reflector for neutron flux, the reaction rates of the ^{115}In(n,n')^{115m}In reaction for the present target assembly are compared with the data for the bare target [4]. The reaction rate ratios of the present target assembly to the bare target are plotted as a function of the distance from the top of the target in Fig. 13.1. The ratios for the ^{93}Nb(n,2n)^{92m}Nb reaction are also plotted in Fig. 13.2 for comparison. The excitation function of the ^{115}In(n,n')^{115m}In and ^{93}Nb(n,2n)^{92m}Nb reaction covers the neutron energy region of 0.3~10 MeV and 10~20 MeV, respectively. The ratios for the ^{115}In(n,n')^{115m}In reaction were about 1.5 on 12 GeV and 24 GeV and 1.2~3.5 on 1.94 GeV. This shows that the lead-reflector is effective to increase the neutron flux in the energy range of 0.3~10 MeV. The ratios for the ^{93}Nb(n,2n)^{92m}Nb reactions were 1.1~1.2 on 12 GeV and 24 GeV and 1.0~1.1 on 1.94 GeV. The lead-reflector is also effective to slightly increase the neutron flux in the energy range of 10~20 MeV.

4. Summary

The spallation neutron characteristcs of the target assembly composed of mercury and the lead-reflector were studied. The incident proton energy was 1.94, 12 and 24 GeV. The activation method was applied to the measurement. Indium, niobium, aluminum, cobalt, nickel and bismuth were used as activation detectors which cover the threshold energy between 0.33 and 40.9 MeV. The measured reaction rates of 17 kinds of the threshold reactions were compiled in this report. It is shown that the lead-reflector is effective for increasing the neutron flux around the cylindrical surface of the mercury target. It is expected that the reaction rate data will be used to validate the calculation code which is being used to optimize a spallation target system.

Acknowledgements

The author would like to thank the operation team of the AGS. They are also grateful to the staff of the Chemistry Department of Brookhaven National Laboratory for their helpful cooperation on the gamma-ray measurement at the Chemistry Building. The Forschungszentrum Juelich (FZK) team of the ASTE collaboration is greatly appreciated for their manufacturing of the mercury target for this experiment. They are thankful to the spokespersons of the ASTE collaboration, Dr. Jeromo Hastings of Brookhaven National Laboratory, Dr. Guenter Bauer of Paul Scherrer Institute, Dr. John Haines of Oak Ridge National Laboratory, Dr. Yukio Oyama and Prof. Noboru Watanabe of Japan Atomic Energy Research Institute for their coordination of the experiment.

References

(1) The Joint Project Team of JAERI and KEK: JAERI-Tech 99-056, "The Joint Project for High-Intensity Proton Accelerators" (1999).

(2) Appleton B. R.: ICANS-XIV, Proc. 14th Meeting of the International Collaboration on Advanced Neutron Sources , ANL-98/33, June. 1998, p. 32-40 (1998).

(3) Niita K., Nara Y., Takada H., Nakashima H., Chiba S. and Ikeda Y.: JAERI-Tech 99-065, "Analysis of the Proton-Induced Reactions at 150 MeV-24 GeV by High Energy Nuclear Reaction Code JAM" (1999). [in Japanese]

(4) Takada H., Kasugai Y., Nakashima H., Ikeda Y., Ino T., Kawai M., Jerde E. and Glasgow D.: JAERI-DATA/Code 2000-008, "Measurement of Activation Reaction Rate Distribution on a Mercury Target Bombardment with High-Energy Protons at AGS" (2000).

(5) Kasugai Y., Takada H. and Ikeda Y.: Proc. of the 10th Int. Symposium on Reactor Dosimetry, to be published.

(6) Kikuchi K., Nakashima H., Ishikura S., Futakawa M. and Hino R.: J. Nucl. Sci. Technol., 37, 113 (2000).

(7) Nakashima H., Takada H., Meigo S., Kasugai Y., Ikeda Y., Oyama Y., Watanabe N. and ASTE collaboration: ICANS-XIV, Proc. 14th Meeting of the International Collaboration on Advanced Neutron Sources , ANL, June. 1998, p. 457-467 (1998).

(8) Takada H., Kasugai Y., Nakashima H., Ikeda Y., Oyama Y., Watanbe N., Arai M., Kiyanagi Y. and ASTE Collaboration: ICANS-XIV, Proc. 14th Meeting of the International Collaboration on Advanced Neutron Sources, ANL, June. 1998, p. 468-477 (1998).

(9) Bauer G. S., Spitzer H., Holzen G., Ni L. and Hasting J.: ICANS-XIV, Proc. 14th Meeting of the International Collaboration on Advanced Neutron Sources , ANL, June. 1998, p. 229-243 (1998).

(10) Futakawa F., Kikuchi K., Conra H., and Stechemesse H.: ICANS-XIV, Proc. 14th Meeting of the International Collaboration on Advanced Neutron Sources, ANL, June. 1998, p. 244-251 (1998).

(11) Meigo S., Nakashima H., Takada H., Kasugai Y., Ino T., Mekawa F. and Hastings J.: to be published in JAERI-Data/Code.

(12) Firestone R. B., Shirley, V. S. (Eds.): "Table of Isotopes 8th Edition", Johon Wiley & Sons Inc., N.Y., (1996).

Table 1 List of the characters of activation detector foils

Material	Purity (%)	Weight (g)	Size (mm)	Thickness (mm)	Impurity
In	99.99	0.25	20×20	0.1	
Nb	99.95	3.4	20×20	1	Fe (20), W (<100), Si (20) Mo (<50), Zr (<100), Ta (900) C(50), O(<100), N(40), H(10) [a]
Al	99.99	1.1	20×20	1	Cu (29), Fe (13), Mg (8) Si (<50) [a]
Co	99.9	3.8	20×20	1	C (0.001), Si (<0.001) Fe (0.005), Cu (0.005) Zr (<100), Ta (900) [b] Ni(0.06), P (0.002) S (0.001) [a]
Ni	99.9	3.5	20×20	1	
Bi	99.9	2.5	15ϕ	1.5	Cu (0.004), Ag(0.001) [b] Fe, Pb(<0.001), others (0.008) [b]

[a] in ppm
[b] in wt%

Table 2 List of the reactions and associated decay data [a]

Reaction			Q-value (MeV)	Eth [b] (MeV)	Half-life	Energy (keV)	Intensity [c] (%)
^{27}Al	(n,α)	^{24}Na	-3.13	3.25	14.959 h	1368.6	100
^{59}Co	(n,γ)	^{60}Co	5.07	0.0	5.2714 y	1173.2	99.9736(7)
	(n,p)	^{59}Fe	-0.78	0.80	44.503 d	1099.3	56.5(15)
	(n,α)	^{56}Mn	0.33	0.0	2.5785 h	845.8	98.9(3)
	(n,2n)	^{58}Co	-10.45	10.63	70.82 d	810.8	99.4
	(n,3n)	^{57}Co	-19.03	19.36	271.79 d	122.1	85.6(2)
	(n,4n)	^{56}Co	-30.40	30.95	77.27 d	846.8	99.940(25)
	(n,5n)	^{55}Co	-40.94	41.22	17.53 h	931.3	75(4)
^{nat}Ni	(n,x)	^{58}Co	0.40 [d]	0.0 [d]	70.82 d	810.8	99.4
	(n,x)	^{57}Co	-8.17 [e]	8.31[e]	271.79 d	122.1	85.6(2)
^{115}In	(n,n')	^{115m}In	-0.34	0.34	4.486 h	336.2	45.9(23)
^{93}Nb	(n,2n)	^{92m}Nb	-8.97	9.06	10.15 d	934.5	99.07(4)
	(n,4n)	^{90}Nb	-28.76	29.08	14.60 h	1129.0	92.7(5)
^{209}Bi	(n,4n)	^{206}Bi	-22.45	22.56	6.243 d	803.1	98.9(1)
	(n,5n)	^{205}Bi	-29.48	29.63	15.31 d	703.4	31.1(1)
	(n,6n)	^{204}Bi	-37.90	38.08	11.22 h	984.0	58.8(4)
	(n,7n)	^{203}Bi	-45.12	45.34	11.76 h	820.3	29.6(15)

[a] Decay data were taken from Table of Isotopes, 8th Edition.
[b] Threshold Energy
[c] For the gamma-ray emission rate, the uncertainty of the last numerical values is given in the parentheses.
[d] for the ^{58}Ni(n,p)^{58}Co reaction.
[e] for the ^{58}Ni(n,np)^{57}Co reaction.

Table 3 Parameters of the proton bombardment

E_{proton}(GeV) [a]	N_{proton} [b]	N_{pluse} [c]	Time (s) [d]
1.94	7.0E+13	56	222
12	4.5E+13	44	394
24	2.1E+13	18	120

[a] Proton Energy
[b] The number of protons
[c] The number of pulses
[d] Time between the first and the last pulse bombardment

Table 4 Major sources of errors in the reaction rates

Source	Error (%)	Correlation [a]
Gamma ray counting statistics	1~20	
Sample weight	0.1	sys
Number of protons	3	sys
Detector efficiency	3~4	sys
Decay Data		sys
Half-life	0~6	sys
Gamma-ray Intensity	0~5	sys

[a] Systematic errors are indicated as "sys".

Table 5 Numerical values for the measured reaction rates

<<Table format for the $^{115}In(n,n')^{115m}In$ reaction on the Main bar>>

Distance [a] (cm)	Reaction rate (attached) [b] (/target nucleus/proton)	δ_{sta} [c]	δ_{tot} [d]	Reaction rate (upward) [b] (/target nucleus/proton)	δ_{sta} [c]	δ_{tot} [d]
0	1.76E-27 [e]	4.0%	7.7%			
1	1.81E-27	4.1%	7.8%	2.04E-27	3.6%	7.5%
•	•	•	•	•	•	•
•	•	•	•	•	•	•
•	•	•	•	•	•	•
•	•	•	•	•	•	•
					δ_{sys}=10% [f]	

<<Table Format for others>>

Distance [a] (cm)	Reaction Rate (/target nucleus/proton)	δ_{sta} [c]	δ_{tot} [d]
9	2.78E-28 [e]	3.4%	5.4%
•	•	•	•
•	•	•	•
•	•	•	•
		δ_{sys}=10% [f]	

[a] Distance from the front-end of the mercury target.
[b] The positions of the indium samples for the acrylic-bar were indicated as "attached" or "upward" for the surface of the bar.
[c] Statistical errors
[d] Total errors including statistical and systematic errors
[e] Reads as 1.76×10^{-27}.
[f] Systematic error

Table 5.1.1 Reaction rates of the $^{115}In(n,n')^{115m}In$ reaction on the Main bar for 1.94 GeV proton bombardment.

Distance [a] (cm)	Reaction rate (attached) (/target nucleus/proton)	δ_{sta}	δ_{tot}	Reaction rate (upward) (/target nucleus/proton)	δ_{sta}	δ_{tot}
-1	1.76E-27	4.0%	7.7%			
1	1.81E-27	4.1%	7.8%	2.04E-27	3.6%	7.5%
5	2.01E-27	3.9%	7.7%	2.21E-27	3.6%	7.5%
9	2.19E-27	3.6%	7.5%	2.56E-27	3.1%	7.3%
13	2.39E-27	3.4%	7.4%			
17	2.14E-27	3.6%	7.5%	2.36E-27	3.3%	7.4%
21	1.95E-27	3.7%	7.6%			
25	1.74E-27	4.1%	7.8%			
27	1.53E-27	4.7%	8.1%	1.78E-27	3.0%	7.2%
33	1.27E-27	4.0%	7.7%			
37	1.02E-27	4.6%	8.1%			
41	9.08E-28	4.2%	7.8%			
45	7.26E-28	4.8%	8.2%			
50	5.53E-28	3.1%	7.3%			
55	3.30E-28	4.5%	8.0%	4.35E-28	3.4%	7.4%
65	2.10E-28	4.3%	7.9%			
75	1.12E-28	5.4%	8.5%			
80	8.12E-29	5.0%	8.3%	8.57E-29	4.4%	7.9%
85	7.39E-29	4.9%	8.2%			
95	4.15E-29	5.0%	8.3%			
100	3.44E-29	5.0%	8.3%	3.64E-29	5.0%	8.3%
					δ_{sys}=6.6%	

Table 5.1.2 Reaction rates of the $^{115}In(n,n')^{115m}In$ reaction on the Sub-1 bar for 1.94 GeV proton bombardment.

Distance (cm)	Reaction Rate (/target nucleus/proton)	δ_{sta}	δ_{tot}
-1	1.65E-27	4.3%	7.9%
5	1.91E-27	4.0%	7.7%
9	2.05E-27	3.6%	7.5%
17	2.04E-27	3.6%	7.5%
21	1.94E-27	3.8%	7.6%
27	1.40E-27	2.4%	7.0%
33	1.20E-27	4.0%	7.7%
45	6.92E-28	4.9%	8.2%
50	5.37E-28	3.9%	7.7%
55	4.01E-28	3.4%	7.4%
75	1.17E-28	5.0%	8.3%
80	9.11E-29	4.9%	8.2%
85	6.50E-29	4.9%	8.2%
		δ_{sys}=6.6%	

Table 5.1.3 Reaction rates of the $^{115}In(n,n')^{115m}In$ reaction on the Sub-2 bar for 1.94 GeV proton bombardment.

Distance (cm)	Reaction Rate (/target nucleus/proton)	δ_{sta}	δ_{tot}
-1	1.77E-27	4.2%	7.8%
5	2.38E-27	3.4%	7.4%
9	2.67E-27	3.2%	7.3%
17	2.48E-27	3.3%	7.4%
21	2.33E-27	3.5%	7.5%
27	1.67E-27	3.5%	7.5%
33	1.35E-27	3.9%	7.7%
45			
50	5.44E-28	3.1%	7.3%
55	4.17E-28	3.7%	7.6%
75	1.08E-28	4.4%	7.9%
80	8.73E-29	5.0%	8.3%
85	6.59E-29	4.9%	8.2%
		δ_{sys}=6.6%	

Table 5.1.4 Reaction rates of the $^{115}In(n,n')^{115m}In$ reaction on the Sub-3 bar for 1.94 GeV proton bombardment.

Distance (cm)	Reaction Rate (/target nucleus/proton)	δ_{sta}	δ_{tot}
-1	2.05E-27	3.6%	7.5%
5	2.45E-27	3.3%	7.4%
9	2.66E-27	3.1%	7.3%
17	2.33E-27	3.6%	7.5%
21	2.22E-27	3.6%	7.5%
27	1.82E-27	3.4%	7.4%
33	1.27E-27	4.2%	7.8%
45	6.19E-28	5.7%	8.7%
50	5.24E-28	3.3%	7.4%
55	3.43E-28	4.3%	7.9%
75	1.18E-28	4.9%	8.2%
80	8.44E-29	5.0%	8.3%
85	6.25E-29	5.0%	8.3%
95	4.11E-29	4.9%	8.2%
100	3.76E-29	5.0%	8.3%
		δ_{sys}=6.6%	

Table 5.1.5 Reaction rates of the $^{115}In(n,n')^{115m}In$ reaction on the Main bar for 12 GeV proton bombardment.

Distance [a] (cm)	Reaction rate (attached) (/target nucleus/proton)	δ_{sta}	δ_{tot}	Reaction rate (upward) (/target nucleus/proton)	δ_{sta}	δ_{tot}
-1	6.38E-27	3.1%	7.3%			
1	7.47E-27	2.8%	7.2%	7.75E-27	2.6%	7.1%
5	7.88E-27	2.7%	7.1%	8.79E-27	2.5%	7.1%
9	9.19E-27	2.5%	7.1%	1.05E-26	2.2%	7.0%
13	1.05E-26	2.4%	7.0%			
17	1.05E-26	2.3%	7.0%	1.17E-26	2.2%	7.0%
21	1.07E-26	2.3%	7.0%			
25	1.06E-26	2.3%	7.0%			
27	1.00E-26	2.4%	7.0%	1.08E-26	2.3%	7.0%
33	8.84E-27	2.6%	7.1%			
37	8.22E-27	2.6%	7.1%			
41	7.17E-27	2.8%	7.2%			
45	5.97E-27	3.2%	7.3%			
50	4.84E-27	1.4%	6.7%			
55	3.70E-27	2.5%	7.0%	4.25E-27	2.7%	7.1%
65	2.47E-27	3.0%	7.2%			
75	1.36E-27	3.0%	7.2%			
80	9.69E-28	3.0%	7.2%	1.25E-27	2.9%	7.2%
85	7.99E-28	3.0%	7.2%			
95	5.06E-28	3.0%	7.2%			
100	3.73E-28	2.9%	7.2%	4.17E-28	0.1%	6.6%
					δ_{sys}=6.6%	

Table 5.1.6 Reaction rates of the $^{115}In(n,n')^{115m}In$ reaction on the Sub-1 bar for 12 GeV proton bombardment.

Distance (cm)	Reaction Rate (/target nucleus/proton)	δ_{sta}	δ_{tot}
-1	6.28E-27	3.2%	7.3%
5	7.21E-27	3.0%	7.2%
9	8.54E-27	2.8%	7.2%
17	9.77E-27	2.6%	7.1%
21	9.66E-27	2.5%	7.1%
27	9.04E-27	2.6%	7.1%
33	8.13E-27	2.7%	7.1%
45	5.68E-27	3.2%	7.4%
50	4.83E-27	2.7%	7.1%
55	3.89E-27	2.8%	7.2%
75	1.41E-27	2.8%	7.2%
80	1.03E-27	2.7%	7.1%
85	8.07E-28	2.9%	7.2%
		δ_{sys} =6.6%	

Table 5.1.7 Reaction rates of the $^{115}In(n,n')^{115m}In$ reaction on the Sub-2 bar for 12 GeV proton bombardment.

Distance (cm)	Reaction Rate (/target nucleus/proton)	δ_{sta}	δ_{tot}
-1	7.69E-27	2.8%	7.2%
5	1.02E-26	2.4%	7.0%
9	1.18E-26	2.3%	7.0%
17	1.33E-26	2.2%	7.0%
21	1.26E-26	2.2%	7.0%
27	1.11E-26	2.4%	7.0%
33	9.51E-27	2.6%	7.1%
45	6.23E-27	3.3%	7.4%
50	5.41E-27	2.9%	7.2%
55	4.19E-27	2.9%	7.2%
75	1.43E-27	2.8%	7.2%
80	1.14E-27	3.0%	7.2%
85	8.05E-28	2.9%	7.2%
		δ_{sys} =6.6%	

Table 5.1.8 Reaction rates of the $^{115}In(n,n')^{115m}In$ reaction on the Sub-3 bar for 12 GeV proton bombardment.

Distance (cm)	Reaction Rate (/target nucleus/proton)	δ_{sta}	δ_{tot}
-1	8.38E-27	2.7%	7.1%
5	1.11E-26	2.4%	7.0%
9	1.22E-26	2.3%	7.0%
17	1.40E-26	2.2%	6.9%
21	1.34E-26	2.2%	7.0%
27	1.22E-26	2.3%	7.0%
33	1.02E-26	2.5%	7.1%
45	7.07E-27	3.0%	7.3%
50	5.12E-27	2.9%	7.2%
55	4.46E-27	3.0%	7.2%
75	1.41E-27	2.9%	7.2%
80	1.09E-27	3.0%	7.2%
85	7.79E-28	2.8%	7.2%
95	4.57E-28	3.0%	7.2%
100	3.94E-28	2.7%	7.1%
		δ_{sys} =6.6%	

Table 5.1.9 Reaction rates of the $^{115}In(n,n')^{115m}In$ reaction on the Main bar for 24 GeV proton bombardment.

Distance [a] (cm)	Reaction rate (attached) (/target nucleus/proton)	δ_{sta}	δ_{tot}	Reaction rate (upward) (/target nucleus/proton)	δ_{sta}	δ_{tot}
-1	9.38E-27	2.1%	6.9%			
1	9.73E-27	2.3%	7.0%	1.19E-26	2.0%	6.9%
5	1.24E-26	2.7%	7.1%	1.39E-26	2.5%	7.0%
9	1.39E-26	2.5%	7.1%	1.61E-26	2.3%	7.0%
13	1.72E-26	2.3%	7.0%			
17	1.67E-26	2.3%	7.0%	1.97E-26	2.1%	6.9%
21	1.84E-26	2.2%	6.9%			
25	1.77E-26	2.2%	7.0%			
27	1.60E-26	2.4%	7.0%	1.87E-26	2.2%	6.9%
33	1.55E-26	2.4%	7.0%			
37	1.38E-26	2.5%	7.1%			
41	1.31E-26	2.6%	7.1%			
45	1.10E-26	3.0%	7.2%			
50	9.42E-27	2.5%	7.1%			
55	7.56E-27	2.9%	7.2%	8.62E-27	2.5%	7.1%
65	5.23E-27	3.0%	7.2%			
75	3.10E-27	2.5%	7.0%			
80	2.27E-27	2.9%	7.2%	2.54E-27	2.6%	7.1%
85	1.99E-27	2.5%	7.1%			
95	1.15E-27	3.0%	7.2%			
100	9.01E-28	3.5%	7.5%	1.10E-27	3.0%	7.2%
					δ_{sys}=6.6%	

Table 5.1.10 Reaction rates of the $^{115}In(n,n')^{115m}In$ reaction on the Sub-1 bar for 24 GeV proton bombardment.

Distance (cm)	Reaction Rate (/target nucleus/proton)	δ_{sta}	δ_{tot}
-1	9.08E-27	3.4%	7.4%
5	1.15E-26	3.0%	7.2%
9	1.38E-26	2.7%	7.1%
17	1.57E-26	2.5%	7.1%
21	1.64E-26	2.5%	7.1%
27	1.55E-26	2.6%	7.1%
33	1.41E-26	2.7%	7.1%
45	1.12E-26	2.7%	7.1%
50	9.09E-27	2.9%	7.2%
55	7.56E-27	3.0%	7.2%
75	3.12E-27	3.0%	7.2%
80	2.37E-27	2.7%	7.1%
85	1.83E-27	3.0%	7.2%
		δ_{sys} =6.6%	

Table 5.1.11 Reaction rates of the $^{115}In(n,n')^{115m}In$ reaction on the Sub-2 bar for 24 GeV proton bombardment.

Distance (cm)	Reaction Rate (/target nucleus/proton)	δ_{sta}	δ_{tot}
-1	1.11E-26	3.1%	7.3%
5	1.50E-26	2.6%	7.1%
9	1.83E-26	2.4%	7.0%
17	2.26E-26	2.1%	6.9%
21	2.22E-26	1.4%	6.7%
27	2.06E-26	2.2%	7.0%
33	1.85E-26	2.4%	7.0%
45	1.25E-26	2.9%	7.2%
50	1.03E-26	3.0%	7.2%
55	8.70E-27	2.5%	7.1%
75	3.43E-27	2.8%	7.2%
80	2.53E-27	2.8%	7.2%
85	2.07E-27	2.9%	7.2%
		δ_{sys} =6.6%	

Table 5.1.12 Reaction rates of the $^{115}In(n,n')^{115m}In$ reaction on the Sub-3 bar for 24 GeV proton bombardment.

Distance (cm)	Reaction Rate (/target nucleus/proton)	δ_{sta}	δ_{tot}
-1	1.13E-26	3.1%	7.3%
5	1.52E-26	2.7%	7.1%
9	1.83E-26	2.4%	7.0%
17	2.26E-26	1.4%	6.7%
21	2.26E-26	2.2%	6.9%
27	2.21E-26	1.5%	6.8%
33	1.96E-26	2.4%	7.0%
45	1.36E-26	3.0%	7.2%
50	1.10E-26	3.0%	7.2%
55	9.39E-27	3.0%	7.2%
75	3.60E-27	3.0%	7.2%
80	2.57E-27	3.0%	7.2%
85	2.10E-27	2.9%	7.2%
95	1.24E-27	3.2%	7.4%
100	1.03E-27	3.6%	7.5%
		δ_{sys} =6.6%	

Table 5.2.1 Reaction rates of the $^{93}Nb(n,2n)^{92m}Nb$ reaction on the Main bar for 1.94 GeV proton bombardment.

Distance (cm)	Reaction Rate (/target nucleus/proton)	δ_{sta}	δ_{tot}
1	2.12E-28	2.9%	5.1%
5	2.40E-28	2.6%	5.0%
9	2.64E-28	2.5%	4.9%
17	2.53E-28	3.1%	5.3%
27	1.57E-28	3.0%	5.2%
55	4.09E-29	5.0%	6.5%
80	9.66E-30	4.8%	6.4%
100	3.96E-30	2.9%	5.1%
		δ_{sys} =4.2%	

Table 5.2.2 Reaction rates of the $^{93}Nb(n,2n)^{92m}Nb$ reaction on the Sub-1 bar for 1.94 GeV proton bombardment.

Distance (cm)	Reaction Rate (/target nucleus/proton)	δ_{sta}	δ_{tot}
9	2.78E-28	3.4%	5.4%
17	2.48E-28	3.2%	5.3%
27	1.78E-28	3.0%	5.2%
55	4.27E-29	4.9%	6.5%
		δ_{sys} =4.2%	

Table 5.2.3 Reaction rates of the $^{93}Nb(n,2n)^{92m}Nb$ reaction on the Sub-2 bar for 1.94 GeV proton bombardment.

Distance (cm)	Reaction Rate (/target nucleus/proton)	δ_{sta}	δ_{tot}
9	3.47E-28	3.0%	5.2%
17	3.20E-28	3.0%	5.2%
27	2.04E-28	3.0%	5.2%
55	4.63E-29	4.9%	6.5%
		δ_{sys} =4.2%	

Table 5.2.4 Reaction rates of the $^{93}Nb(n,2n)^{92m}Nb$ reaction on the Sub-3 bar for 1.94 GeV proton bombardment.

Distance (cm)	Reaction Rate (/target nucleus/proton)	δ_{sta}	δ_{tot}
9	3.11E-28	2.7%	5.1%
17	3.11E-28	2.8%	5.1%
27	1.90E-28	2.9%	5.1%
55	4.27E-29	3.5%	5.5%
		δ_{sys} =4.2%	

Table 5.2.5 Reaction rates of the $^{93}Nb(n,2n)^{92m}Nb$ reaction on the Main bar for 12 GeV proton bombardment.

Distance (cm)	Reaction Rate (/target nucleus/proton)	δ_{sta}	δ_{tot}
1	7.67E-28	2.9%	5.2%
5	9.33E-28	3.0%	5.2%
9	1.07E-27	3.0%	5.2%
17	1.19E-27	2.9%	5.1%
27	1.03E-27	3.0%	5.2%
55	4.12E-28	3.1%	5.2%
80	1.21E-28	3.0%	5.2%
100	4.12E-29	4.9%	6.4%
		δ_{sys} =4.2%	

Table 5.2.6 Reaction rates of the $^{93}Nb(n,2n)^{92m}Nb$ reaction on the Sub-1 bar for 12 GeV proton bombardment.

Distance (cm)	Reaction Rate (/target nucleus/proton)	δ_{sta}	δ_{tot}
9	9.51E-28	1.9%	4.7%
17	1.09E-27	2.7%	5.0%
27	9.84E-28	3.0%	5.2%
55	3.82E-28	3.2%	5.3%
		δ_{sys} =4.2%	

Table 5.2.7 Reaction rates of the $^{93}Nb(n,2n)^{92m}Nb$ reaction on the Sub-2 bar for 12 GeV proton bombardment.

Distance (cm)	Reaction Rate (/target nucleus/proton)	δ_{sta}	δ_{tot}
9	1.53E-27	2.9%	5.2%
17	1.67E-27	2.9%	5.1%
27	1.41E-27	2.9%	5.1%
55	4.99E-28	2.9%	5.2%
		δ_{sys} =4.2%	

Table 5.2.8 Reaction rates of the $^{93}Nb(n,2n)^{92m}Nb$ reaction on the Sub-3 bar for 12 GeV proton bombardment.

Distance (cm)	Reaction Rate (/target nucleus/proton)	δ_{sta}	δ_{tot}
9	1.60E-27	3.0%	5.2%
17	1.71E-27	2.7%	5.1%
27	1.50E-27	2.9%	5.1%
55	5.47E-28	3.0%	5.2%
		δ_{sys} =4.2%	

Table 5.2.9 Reaction rates of the $^{93}Nb(n,2n)^{92m}Nb$ reaction on the Main bar for 24 GeV proton bombardment.

Distance (cm)	Reaction Rate (/target nucleus/proton)	δ_{sta}	δ_{tot}
1	1.10E-27	3.0%	5.2%
5	1.25E-27	2.8%	5.1%
9	1.46E-27	2.7%	5.0%
17	1.98E-27	2.6%	5.0%
27	1.67E-27	3.0%	5.2%
55	8.59E-28	3.0%	5.2%
80	2.67E-28	4.4%	6.1%
100	9.85E-29	3.9%	5.8%
		δ_{sys} =4.2%	

Table 5.2.10 Reaction rates of the $^{93}Nb(n,2n)^{92m}Nb$ reaction on the Sub-1 bar for 24 GeV proton bombardment.

Distance (cm)	Reaction Rate (/target nucleus/proton)	δ_{sta}	δ_{tot}
9	1.35E-27	2.9%	5.1%
17	1.75E-27	3.0%	5.2%
27	1.61E-27	2.1%	4.8%
55	7.42E-28	3.2%	5.3%
		δ_{sys} =4.2%	

Table 5.2.11 Reaction rates of the $^{93}Nb(n,2n)^{92m}Nb$ reaction on the Sub-2 bar for 24 GeV proton bombardment.

Distance (cm)	Reaction Rate (/target nucleus/proton)	δ_{sta}	δ_{tot}
9	2.22E-27	2.4%	4.9%
17	2.55E-27	2.9%	5.1%
27	2.79E-27	2.8%	5.1%
55	9.45E-28	2.8%	5.1%
		δ_{sys} =4.2%	

Table 5.2.12 Reaction rates of the $^{93}Nb(n,2n)^{92m}Nb$ reaction on the Sub-3 bar for 24 GeV proton bombardment.

Distance (cm)	Reaction Rate (/target nucleus/proton)	δ_{sta}	δ_{tot}
9	2.04E-27	2.7%	5.0%
17	2.63E-27	2.7%	5.0%
27	2.50E-27	2.9%	5.1%
55	1.02E-27	3.0%	5.2%
		δ_{sys} =4.2%	

Table 5.3.1 Reaction rates of the $^{93}Nb(n,4n)^{92m}Nb$ reaction on the Main bar for 1.94 GeV proton bombardment.

Distance (cm)	Reaction Rate (/target nucleus/proton)	δ_{sta}	δ_{tot}
1	7.54E-29	4.7%	6.3%
5	9.15E-29	4.5%	6.2%
9	1.15E-28	4.0%	5.8%
17	1.08E-28	4.8%	6.4%
27	8.21E-29	4.2%	6.0%
55	2.04E-29	6.8%	8.0%
80	5.91E-30	9.3%	10.2%
100	2.65E-30	4.0%	5.8%
		δ_{sys} =4.2%	

Table 5.3.2 Reaction rates of the $^{93}Nb(n,4n)^{92m}Nb$ reaction on the Sub-1 bar for 1.94 GeV proton bombardment.

Distance (cm)	Reaction Rate (/target nucleus/proton)	δ_{sta}	δ_{tot}
9	1.08E-28	5.6%	7.0%
17	1.09E-28	5.0%	6.6%
27	8.23E-29	4.8%	6.4%
55	2.56E-29	5.9%	7.3%
		δ_{sys} =4.2%	

Table 5.3.3 Reaction rates of the $^{93}Nb(n,4n)^{92m}Nb$ reaction on the Sub-2 bar for 1.94 GeV proton bombardment.

Distance (cm)	Reaction Rate (/target nucleus/proton)	δ_{sta}	δ_{tot}
9	1.48E-28	4.4%	6.1%
17	1.47E-28	4.6%	6.3%
27	1.02E-28	4.3%	6.0%
55	2.50E-29	6.0%	7.3%
		δ_{sys} =4.2%	

Table 5.3.4 Reaction rates of the $^{93}Nb(n,4n)^{92m}Nb$ reaction on the Sub-3 bar for 1.94 GeV proton bombardment.

Distance (cm)	Reaction Rate (/target nucleus/proton)	δ_{sta}	δ_{tot}
9	1.35E-28	6.2%	7.5%
17	1.28E-28	6.6%	7.8%
27	9.03E-29	6.6%	7.8%
55	2.25E-29	7.0%	8.2%
		δ_{sys} =4.2%	

Table 5.3.5 Reaction rates of the $^{93}Nb(n,4n)^{92m}Nb$ reaction on the Main bar for 12 GeV proton bombardment.

Distance (cm)	Reaction Rate (/target nucleus/proton)	δ_{sta}	δ_{tot}
1	2.67E-28	5.0%	6.6%
5	3.04E-28	5.1%	6.6%
9	3.81E-28	4.6%	6.3%
17	5.31E-28	4.0%	5.8%
27	4.44E-28	3.9%	5.8%
55	1.87E-28	4.5%	6.2%
80	6.15E-29	5.1%	6.6%
100	2.27E-29	8.4%	9.4%
		δ_{sys} =4.2%	

Table 5.3.6 Reaction rates of the $^{93}Nb(n,4n)^{92m}Nb$ reaction on the Sub-1 bar for 12 GeV proton bombardment.

Distance (cm)	Reaction Rate (/target nucleus/proton)	δ_{sta}	δ_{tot}
9	5.28E-28	5.1%	6.6%
17	6.76E-28	4.4%	6.1%
27	6.25E-28	4.4%	6.1%
55	2.22E-28	3.9%	5.8%
		δ_{sys} =4.2%	

Table 5.3.7 Reaction rates of the $^{93}Nb(n,4n)^{92m}Nb$ reaction on the Sub-2 bar for 12 GeV proton bombardment.

Distance (cm)	Reaction Rate (/target nucleus/proton)	δ_{sta}	δ_{tot}
9	3.63E-28	3.3%	5.4%
17	4.42E-28	4.2%	6.0%
27	3.98E-28	4.6%	6.3%
55	1.71E-28	4.8%	6.4%
		δ_{sys} =4.2%	

Table 5.3.8 Reaction rates of the $^{93}Nb(n,4n)^{92m}Nb$ reaction on the Sub-2 bar for 12 GeV proton bombardment.

Distance (cm)	Reaction Rate (/target nucleus/proton)	δ_{sta}	δ_{tot}
9	6.11E-28	4.8%	6.4%
17	7.04E-28	4.1%	5.9%
27	6.07E-28	4.6%	6.3%
55	2.28E-28	4.5%	6.2%
		δ_{sys} =4.2%	

Table 5.3.9 Reaction rates of the $^{93}Nb(n,4n)^{92m}Nb$ reaction on the Main bar for 24 GeV proton bombardment.

Distance (cm)	Reaction Rate (/target nucleus/proton)	δ_{sta}	δ_{tot}
1	4.27E-28	5.4%	6.9%
5	4.98E-28	4.7%	6.3%
9	6.12E-28	4.8%	6.4%
17	9.10E-28	4.3%	6.0%
27	8.15E-28	4.9%	6.5%
55	4.14E-28	5.5%	6.9%
80	1.30E-28	7.1%	8.3%
100	5.53E-29	7.3%	8.4%
		δ_{sys} =4.2%	

Table 5.3.10 Reaction rates of the $^{93}Nb(n,4n)^{92m}Nb$ reaction on the Sub-1 bar for 24 GeV proton bombardment.

Distance (cm)	Reaction Rate (/target nucleus/proton)	δ_{sta}	δ_{tot}
9	6.00E-28	4.9%	6.5%
17	7.48E-28	5.2%	6.7%
27	6.72E-28	4.1%	5.9%
55	3.78E-28	6.3%	7.6%
		δ_{sys} =4.2%	

Table 5.3.11 Reaction rates of the $^{93}Nb(n,4n)^{92m}Nb$ reaction on the Sub-2 bar for 24 GeV proton bombardment.

Distance (cm)	Reaction Rate (/target nucleus/proton)	δ_{sta}	δ_{tot}
9	9.10E-28	4.4%	6.1%
17	1.12E-27	5.8%	7.2%
27	1.14E-27	5.1%	6.6%
55	4.79E-28	5.3%	6.8%
		δ_{sys} =4.2%	

Table 5.3.12 Reaction rates of the $^{93}Nb(n,4n)^{92m}Nb$ reaction on the Sub-3 bar for 24 GeV proton bombardment.

Distance (cm)	Reaction Rate (/target nucleus/proton)	δ_{sta}	δ_{tot}
9	9.41E-28	4.9%	6.5%
17	1.21E-27	5.0%	6.6%
27	1.12E-27	5.5%	6.9%
55	5.02E-28	5.7%	7.1%
		δ_{sys} =4.2%	

Table 5.4.1 Reaction rates of the $^{27}Al(n,\alpha)^{24}Na$ reaction on the main bar for 1.94 GeV proton bombardment.

Distance (cm)	Reaction Rate (/target nucleus/proton)	δ_{sta}	δ_{tot}
1	8.50E-29	0.6%	5.0%
5	9.25E-29	0.6%	5.0%
9	1.04E-28	0.6%	5.0%
17	9.74E-29	0.6%	5.0%
27	6.60E-29	0.7%	5.0%
55	1.52E-29	1.4%	5.2%
80	3.61E-30	3.0%	5.8%
100	1.50E-30	4.8%	6.9%
		δ_{sys} =5.0%	

Table 5.4.2 Reaction rates of the $^{27}Al(n,\alpha)^{24}Na$ reaction on the main bar for 12 GeV proton bombardment.

Distance (cm)	Reaction Rate (/target nucleus/proton)	δ_{sta}	δ_{tot}
1	2.45E-28	0.5%	5.0%
5	2.87E-28	0.4%	5.0%
9	3.38E-28	0.4%	5.0%
17	3.85E-28	0.4%	5.0%
27	3.55E-28	0.4%	5.0%
55	1.32E-28	0.6%	5.0%
80	3.87E-29	1.1%	5.1%
100	1.40E-29	1.9%	5.3%
		δ_{sys} =5.0%	

Table 5.4.3 Reaction rates of the $^{27}Al(n,\alpha)^{24}Na$ reaction on the main bar for 1.94 GeV proton bombardment.

Distance (cm)	Reaction Rate (/target nucleus/proton)	δ_{sta}	δ_{tot}
1	3.48E-28	0.7%	5.0%
5	4.40E-28	0.6%	5.0%
9	5.13E-28	0.5%	5.0%
17	6.73E-28	0.5%	5.0%
27	6.21E-28	0.5%	5.0%
55	2.94E-28	0.7%	5.0%
80	9.42E-29	1.0%	5.1%
100	3.66E-29	1.6%	5.2%
		δ_{sys} =5.0%	

Table 5.5.1 Reaction rates of the $^{59}Co(n,\gamma)^{60}Co$ reaction on the main bar for 1.94 GeV proton bombardment.

Distance (cm)	Reaction Rate (/target nucleus/proton)	δ_{sta}	δ_{tot}
1	1.92E-26	0.2%	5.0%
5	1.96E-26	0.2%	5.0%
9	1.94E-26	0.2%	5.0%
17	1.75E-26	0.2%	5.0%
27	1.34E-26	0.3%	5.0%
55	5.80E-27	0.4%	5.0%
80	2.68E-27	0.6%	5.0%
100	2.15E-27	0.7%	5.0%
		δ_{sys} =5.0%	

Table 5.5.2 Reaction rates of the $^{59}Co(n,\gamma)^{60}Co$ reaction on the main bar for 12 GeV proton bombardment.

Distance (cm)	Reaction Rate (/target nucleus/proton)	δ_{sta}	δ_{tot}
1	8.50E-26	0.1%	5.0%
5	8.83E-26	0.1%	5.0%
9	9.69E-26	0.1%	5.0%
17	1.02E-25	0.1%	5.0%
27	8.00E-26	0.1%	5.0%
55	3.45E-26	0.2%	5.0%
80	1.09E-26	0.3%	5.0%
100	6.90E-27	0.5%	5.0%
		δ_{sys} =5.0%	

Table 5.5.3 Reaction rates of the $^{59}Co(n,\gamma)^{60}Co$ reaction on the main bar for 24 GeV proton bombardment.

Distance (cm)	Reaction Rate (/target nucleus/proton)	δ_{sta}	δ_{tot}
1	1.64E-25	0.1%	5.0%
5	1.64E-25	0.1%	5.0%
9	1.69E-25	0.1%	5.0%
17	1.95E-25	0.1%	5.0%
27	1.67E-25	0.1%	5.0%
55	6.96E-26	0.2%	5.0%
80	2.74E-26	0.3%	5.0%
100	1.74E-26	0.4%	5.0%
		δ_{sys} =5.0%	

Table 5.6.1 Reaction rates of the $^{59}Co(n,\alpha)^{56}Mn$ reaction on the main bar for 1.94 GeV proton bombardment.

Distance (cm)	Reaction Rate (/target nucleus/proton)	δ_{sta}	δ_{tot}
1	2.47E-29	0.5%	5.0%
5	2.85E-29	0.5%	5.0%
9	3.24E-29	0.4%	5.0%
17	3.11E-29	0.4%	5.0%
27	2.20E-29	0.5%	5.0%
55	4.93E-30	1.0%	5.1%
80	1.23E-30	1.9%	5.4%
100	5.88E-31	2.7%	5.7%
		δ_{sys} =5.0%	

Table 5.6.2 Reaction rates of the $^{59}Co(n,\alpha)^{56}Mn$ reaction on the main bar for 12 GeV proton bombardment.

Distance (cm)	Reaction Rate (/target nucleus/proton)	δ_{sta}	δ_{tot}
1	7.46E-29	0.4%	5.0%
5	8.92E-29	0.4%	5.0%
9	1.07E-28	0.3%	5.0%
17	1.26E-28	0.3%	5.0%
27	1.16E-28	0.3%	5.0%
55	4.52E-29	0.5%	5.0%
80	1.33E-29	0.8%	5.1%
100	5.06E-30	1.3%	5.2%
		δ_{sys} =5.0%	

Table 5.6.3 Reaction rates of the $^{59}Co(n,\alpha)^{56}Mn$ reaction on the main bar for 24 GeV proton bombardment.

Distance (cm)	Reaction Rate (/target nucleus/proton)	δ_{sta}	δ_{tot}
1	1.12E-28	0.7%	5.1%
5	1.39E-28	0.6%	5.0%
9	1.65E-28	0.5%	5.0%
17	2.11E-28	0.4%	5.0%
27	2.10E-28	0.4%	5.0%
55	9.91E-29	0.5%	5.0%
80	3.48E-29	0.9%	5.1%
100	1.29E-29	1.4%	5.2%
		δ_{sys} =5.0%	

Table 5.7.1 Reaction rates of the $^{59}Co(n,2n)^{58}Co$ reaction on the main bar for 1.94 GeV proton bombardment.

Distance (cm)	Reaction Rate (/target nucleus/proton)	δ_{sta}	δ_{tot}
1	3.91E-28	0.5%	5.0%
5	4.55E-28	0.4%	5.0%
9	5.00E-28	0.4%	5.0%
17	4.73E-28	0.4%	5.0%
27	3.27E-28	0.5%	5.0%
55	7.33E-29	1.3%	5.2%
80	1.76E-29	3.4%	6.1%
100	8.93E-30	4.1%	6.5%
		δ_{sys} =5.0%	

Table 5.7.2 Reaction rates of the $^{59}Co(n,2n)^{58}Co$ reaction on the main bar for 12 GeV proton bombardment.

Distance (cm)	Reaction Rate (/target nucleus/proton)	δ_{sta}	δ_{tot}
1	1.21E-27	0.4%	5.0%
5	1.43E-27	0.3%	5.0%
9	1.69E-27	0.3%	5.0%
17	1.96E-27	0.3%	5.0%
27	1.75E-27	0.3%	5.0%
55	6.73E-28	0.5%	5.0%
80	2.01E-28	0.9%	5.1%
100	7.34E-29	1.5%	5.2%
		δ_{sys} =5.0%	

Table 5.7.3 Reaction rates of the $^{59}Co(n,2n)^{58}Co$ reaction on the main bar for 24 GeV proton bombardment.

Distance (cm)	Reaction Rate (/target nucleus/proton)	δ_{sta}	δ_{tot}
1	1.86E-27	0.5%	5.0%
5	2.28E-27	0.4%	5.0%
9	2.69E-27	0.4%	5.0%
17	3.29E-27	0.3%	5.0%
27	3.21E-27	0.3%	5.0%
55	1.45E-27	0.4%	5.0%
80	4.93E-28	0.8%	5.1%
100	1.94E-28	1.4%	5.2%
		δ_{sys} =5.0%	

Table 5.8.1 Reaction rates of the $^{59}Co(n,3n)^{56}Co$ reaction on the main bar for 1.94 GeV proton bombardment.

Distance (cm)	Reaction Rate (/target nucleus/proton)	δ_{sta}	δ_{tot}
1	8.99E-29	1.3%	5.2%
5	1.06E-28	1.2%	5.1%
9	1.19E-28	1.1%	5.1%
17	1.22E-28	1.0%	5.1%
27	8.52E-29	1.3%	5.2%
55	2.23E-29	3.1%	5.9%
80	6.33E-30	6.9%	8.5%
100	3.70E-30	13.5%	14.4%
		δ_{sys} =5.0%	

Table 5.8.2 Reaction rates of the $^{59}Co(n,3n)^{56}Co$ reaction on the main bar for 12 GeV proton bombardment.

Distance (cm)	Reaction Rate (/target nucleus/proton)	δ_{sta}	δ_{tot}
1	2.86E-28	0.9%	5.1%
5	3.52E-28	0.8%	5.1%
9	4.07E-28	0.7%	5.1%
17	4.96E-28	0.5%	5.0%
27	4.52E-28	0.7%	5.0%
55	1.76E-28	1.1%	5.1%
80	5.47E-29	2.1%	5.4%
100	2.24E-29	3.7%	6.2%
		δ_{sys} =5.0%	

Table 5.8.3 Reaction rates of the $^{59}Co(n,3n)^{56}Co$ reaction on the main bar for 24 GeV proton bombardment.

Distance (cm)	Reaction Rate (/target nucleus/proton)	δ_{sta}	δ_{tot}
1	4.35E-28	1.2%	5.2%
5			
9	6.64E-28	0.9%	5.1%
17	8.28E-28	0.7%	5.0%
27	8.17E-28	0.8%	5.1%
55	4.00E-28	1.1%	5.1%
80	1.35E-28	2.0%	5.4%
100	4.81E-29	4.4%	6.7%
		δ_{sys} =5.0%	

Table 5.9.1 Reaction rates of the $^{59}Co(n,4n)^{56}Co$ reaction on the main bar for 1.94 GeV proton bombardment.

Distance (cm)	Reaction Rate (/target nucleus/proton)	δ_{sta}	δ_{tot}
1	1.26E-29	5.9%	7.7%
5	1.57E-29	4.4%	6.7%
9	1.84E-29	4.4%	6.7%
17	1.85E-29	4.2%	6.5%
27	1.24E-29	4.8%	6.9%
55	3.75E-30	10.5%	11.7%
80	1.87E-30	18.4%	19.0%
100			
		δ_{sys} =5.0%	

Table 5.9.2 Reaction rates of the $^{59}Co(n,4n)^{56}Co$ reaction on the main bar for 12 GeV proton bombardment.

Distance (cm)	Reaction Rate (/target nucleus/proton)	δ_{sta}	δ_{tot}
1	3.64E-29	4.7%	6.9%
5	4.90E-29	3.6%	6.2%
9	5.01E-29	3.5%	6.1%
17	6.85E-29	2.9%	5.8%
27	7.12E-29	2.5%	5.6%
55	2.75E-29	3.6%	6.2%
80	9.05E-30	8.4%	9.8%
100	3.10E-30	19.6%	20.2%
		δ_{sys} =5.0%	

Table 5.9.3 Reaction rates of the $^{59}Co(n,4n)^{56}Co$ reaction on the main bar for 24 GeV proton bombardment.

Distance (cm)	Reaction Rate (/target nucleus/proton)	δ_{sta}	δ_{tot}
1	5.25E-29	7.1%	8.7%
5	8.32E-29	4.4%	6.7%
9	9.35E-29	4.0%	6.4%
17	1.13E-28	3.4%	6.1%
27	1.22E-28	3.0%	5.8%
55	6.40E-29	4.2%	6.5%
80	1.36E-29	12.1%	13.1%
100	1.21E-29	11.2%	12.3%
		δ_{sys} =5.0%	

Table 5.10.1 Reaction rates of the $^{59}Co(n,5n)^{55}Co$ reaction on the main bar for 1.94 GeV proton bombardment.

Distance (cm)	Reaction Rate (/target nucleus/proton)	δ_{sta}	δ_{tot}
1	9.60E-31	11.9%	13.9%
5	1.32E-30	8.4%	11.1%
9	1.75E-30	6.9%	10.0%
17	1.36E-30	7.9%	10.8%
27	1.40E-30	8.9%	11.5%
55	3.10E-31	19.9%	21.2%
80			
100			
		δ_{sys} =7.3%	

Table 5.10.2 Reaction rates of the $^{59}Co(n,5n)^{55}Co$ reaction on the main bar for 12 GeV proton bombardment.

Distance (cm)	Reaction Rate (/target nucleus/proton)	δ_{sta}	δ_{tot}
1	2.61E-30	7.8%	10.7%
5	2.42E-30	10.4%	12.7%
9	4.38E-30	6.6%	9.9%
17	5.89E-30	5.2%	8.9%
27	5.11E-30	5.2%	9.0%
55	2.25E-30	8.5%	11.2%
80	7.56E-31	14.1%	15.9%
100	5.20E-31	18.3%	19.7%
		δ_{sys} =7.3%	

Table 5.10.3 Reaction rates of the $^{59}Co(n,5n)^{55}Co$ reaction on the main bar for 24 GeV proton bombardment.

Distance (cm)	Reaction Rate (/target nucleus/proton)	δ_{sta}	δ_{tot}
1	3.38E-30	14.1%	15.9%
5	4.16E-30	11.2%	13.4%
9	6.11E-30	8.1%	10.9%
17	1.13E-29	6.3%	9.7%
27	9.25E-30	6.4%	9.7%
55	4.98E-30	8.5%	11.2%
80	1.73E-30	14.3%	16.0%
100			
		δ_{sys} =7.3%	

Table 5.11.1 Reaction rates of the $^{nat}Ni(n,x)^{58}Co$ reaction on the main bar for 1.94 GeV proton bombardment.

Distance (cm)	Reaction Rate (/target nucleus/proton)	δ_{sta}	δ_{tot}
1	8.86E-28	0.3%	5.0%
5	9.72E-28	0.3%	5.0%
9	1.06E-27	0.2%	5.0%
17	9.61E-28	0.3%	5.0%
27	6.59E-28	0.3%	5.0%
55	1.46E-28	0.7%	5.0%
80	2.95E-29	1.7%	5.3%
100	1.13E-29	3.4%	6.0%
		δ_{sys} =7.3%	

Table 5.11.2 Reaction rates of the $^{nat}Ni(n,x)^{58}Co$ reaction on the main bar for 12 GeV proton bombardment.

Distance (cm)	Reaction Rate (/target nucleus/proton)	δ_{sta}	δ_{tot}
1	2.60E-27	0.2%	5.0%
5	3.00E-27	0.2%	5.0%
9	3.46E-27	0.2%	5.0%
17	3.98E-27	0.2%	5.0%
27	3.53E-27	0.2%	5.0%
55	1.35E-27	0.3%	5.0%
80	3.75E-28	0.5%	5.0%
100	1.35E-28	0.9%	5.1%
		δ_{sys} =7.3%	

Table 5.11.3 Reaction rates of the $^{nat}Ni(n,x)^{58}Co$ reaction on the main bar for 24 GeV proton bombardment.

Distance (cm)	Reaction Rate (/target nucleus/proton)	δ_{sta}	δ_{tot}
1	4.04E-27	0.2%	5.0%
5	4.80E-27	0.2%	5.0%
9	5.65E-27	0.2%	5.0%
17	6.79E-27	0.2%	5.0%
27	6.50E-27	0.2%	5.0%
55	2.81E-27	0.3%	5.0%
80	9.42E-28	0.5%	5.0%
100	3.62E-28	0.8%	5.1%
		δ_{sys} =7.3%	

Table 5.12.1 Reaction rates of the $^{nat}Ni(n,x)^{57}Co$ reaction on the main bar for 1.94 GeV proton bombardment.

Distance (cm)	Reaction Rate (/target nucleus/proton)	δ_{sta}	δ_{tot}
1	2.87E-28	0.5%	5.0%
5	3.38E-28	0.5%	5.0%
9	3.84E-28	0.4%	5.0%
17	3.64E-28	0.5%	5.0%
27	2.54E-28	0.6%	5.0%
55	5.78E-29	1.3%	5.2%
80	1.51E-29	3.0%	5.8%
100	6.97E-30	5.9%	7.7%
		δ_{sys} =5.0%	

Table 5.12.2 Reaction rates of the $^{nat}Ni(n,x)^{57}Co$ reaction on the main bar for 12 GeV proton bombardment.

Distance (cm)	Reaction Rate (/target nucleus/proton)	δ_{sta}	δ_{tot}
1	8.96E-28	0.3%	5.0%
5	1.08E-27	0.3%	5.0%
9	1.25E-27	0.2%	5.0%
17	1.50E-27	0.3%	5.0%
27	1.35E-27	0.3%	5.0%
55	5.17E-28	0.5%	5.0%
80	1.59E-28	0.9%	5.1%
100	5.58E-29	1.6%	5.3%
		δ_{sys} =5.0%	

Table 5.12.3 Reaction rates of the $^{nat}Ni(n,x)^{57}Co$ reaction on the main bar for 24 GeV proton bombardment.

Distance (cm)	Reaction Rate (/target nucleus/proton)	δ_{sta}	δ_{tot}
1	1.35E-27	0.4%	5.0%
5	1.70E-27	0.4%	5.0%
9	2.04E-27	0.3%	5.0%
17	2.51E-27	0.3%	5.0%
27	2.45E-27	0.3%	5.0%
55	1.08E-27	0.5%	5.0%
80	3.85E-28	0.9%	5.1%
100	1.50E-28	1.5%	5.2%
		δ_{sys} =5.0%	

Table 5.13.1 Reaction rates of the $^{209}Bi(n,4n)^{206}Bi$ reaction on the main bar for 1.94 GeV proton bombardment.

Distance (cm)	Reaction Rate (/target nucleus/proton)	δ_{sta}	δ_{tot}
1	2.78E-28	1.0%	5.1%
5	3.33E-28	0.9%	5.1%
9	3.65E-28	0.6%	5.0%
17	3.63E-28	0.6%	5.0%
27	2.50E-28	0.7%	5.0%
55	5.87E-29	1.7%	5.3%
80	1.51E-29	12.8%	13.8%
100	7.41E-30	26.2%	26.7%
		δ_{sys} =5.0%	

Table 5.13.2 Reaction rates of the $^{209}Bi(n,4n)^{206}Bi$ reaction on the main bar for 12 GeV proton bombardment.

Distance (cm)	Reaction Rate (/target nucleus/proton)	δ_{sta}	δ_{tot}
1	8.64E-28	0.8%	5.1%
5	1.05E-27	0.6%	5.0%
9	1.23E-27	0.2%	5.0%
17	1.49E-27	0.4%	5.0%
27	1.35E-27	0.4%	5.0%
55	5.21E-28	0.6%	5.0%
80	1.57E-28	1.9%	5.4%
100	5.74E-29	5.2%	7.2%
		δ_{sys} =5.0%	

Table 5.13.3 Reaction rates of the $^{209}Bi(n,4n)^{206}Bi$ reaction on the main bar for 24 GeV proton bombardment.

Distance (cm)	Reaction Rate (/target nucleus/proton)	δ_{sta}	δ_{tot}
1	1.33E-27	1.1%	5.1%
5	1.63E-27	0.8%	5.1%
9	1.99E-27	0.7%	5.0%
17	2.33E-27	0.5%	5.0%
27	2.42E-27	0.4%	5.0%
55	1.10E-27	0.6%	5.0%
80	3.90E-28	0.9%	5.1%
100	1.65E-28	4.0%	6.4%
		δ_{sys} =5.0%	

Table 5.14.1 Reaction rates of the $^{209}Bi(n,5n)^{205}Bi$ reaction on the main bar for 1.94 GeV proton bombardment.

Distance (cm)	Reaction Rate (/target nucleus/proton)	δ_{sta}	δ_{tot}
1	1.98E-28	1.8%	5.3%
5	2.39E-28	1.5%	5.2%
9	2.69E-28	1.4%	5.2%
17	2.74E-28	1.3%	5.2%
27	1.90E-28	1.5%	5.2%
55	4.85E-29	4.1%	6.5%
80	1.85E-29	5.8%	7.7%
100	7.06E-30	12.4%	13.4%
		δ_{sys} =5.0%	

Table 5.14.2 Reaction rates of the $^{209}Bi(n,5n)^{205}Bi$ reaction on the main bar for 12 GeV proton bombardment.

Distance (cm)	Reaction Rate (/target nucleus/proton)	δ_{sta}	δ_{tot}
1	6.14E-28	1.2%	5.1%
5	7.46E-28	1.0%	5.1%
9	9.34E-28	0.7%	5.1%
17	1.13E-27	0.7%	5.1%
27	1.03E-27	0.8%	5.1%
55	3.98E-28	1.2%	5.2%
80	1.25E-28	2.5%	5.6%
100	4.63E-29	5.2%	7.2%
		δ_{sys} =5.0%	

Table 5.14.3 Reaction rates of the $^{209}Bi(n,5n)^{205}Bi$ reaction on the main bar for 24 GeV proton bombardment.

Distance (cm)	Reaction Rate (/target nucleus/proton)	δ_{sta}	δ_{tot}
1	9.71E-28	1.6%	5.3%
5	1.17E-27	1.3%	5.2%
9	1.51E-27	1.0%	5.1%
17	1.78E-27	0.9%	5.1%
27	1.89E-27	0.9%	5.1%
55	8.43E-28	1.2%	5.2%
80	3.28E-28	2.1%	5.4%
100	1.24E-28	3.5%	6.1%
		δ_{sys} =5.0%	

Table 5.15.1 Reaction rates of the $^{209}Bi(n,6n)^{204}Bi$ reaction on the main bar for 1.94 GeV proton bombardment.

Distance (cm)	Reaction Rate (/target nucleus/proton)	δ_{sta}	δ_{tot}
1	1.11E-28	0.5%	5.1%
5	1.49E-28	0.4%	5.1%
9	1.78E-28	0.4%	5.1%
17	1.85E-28	0.4%	5.1%
27	1.34E-28	0.5%	5.1%
55	3.24E-29	0.9%	5.1%
80	9.02E-30	1.8%	5.3%
100	4.32E-30	2.8%	5.8%
		δ_{sys} =5.0%	

Table 5.15.2 Reaction rates of the $^{209}Bi(n,6n)^{204}Bi$ reaction on the main bar for 12 GeV proton bombardment.

Distance (cm)	Reaction Rate (/target nucleus/proton)	δ_{sta}	δ_{tot}
1	3.61E-28	0.3%	5.1%
5	4.63E-28	0.3%	5.1%
9	5.64E-28	0.3%	5.1%
17	7.03E-28	0.2%	5.1%
27	6.48E-28	0.2%	5.1%
55	2.64E-28	0.4%	5.1%
80	8.26E-29	0.7%	5.1%
100	3.01E-29	1.2%	5.2%
		δ_{sys} =5.0%	

Table 5.15.3 Reaction rates of the $^{209}Bi(n,6n)^{204}Bi$ reaction on the main bar for 24 GeV proton bombardment.

Distance (cm)	Reaction Rate (/target nucleus/proton)	δ_{sta}	δ_{tot}
1	5.15E-28	0.4%	5.1%
5	6.71E-28	0.4%	5.1%
9	8.59E-28	0.3%	5.1%
17	1.04E-27	0.3%	5.1%
27	1.14E-27	0.3%	5.1%
55	5.04E-28	0.4%	5.1%
80	1.88E-28	0.7%	5.1%
100	7.23E-29	1.1%	5.2%
		δ_{sys} =5.0%	

Table 5.16.1 Reaction rates of the $^{209}Bi(n,7n)^{203}Bi$ reaction on the main bar for 1.94 GeV proton bombardment.

Distance (cm)	Reaction Rate (/target nucleus/proton)	δ_{sta}	δ_{tot}
1	8.00E-29	2.1%	7.4%
5	1.05E-28	1.8%	7.3%
9	1.36E-28	2.0%	7.4%
17	1.29E-28	1.6%	7.3%
27	1.05E-28	1.8%	7.3%
55	2.69E-29	3.6%	8.0%
80	6.38E-30	9.4%	11.8%
100	5.73E-30	7.4%	10.3%
		δ_{sys} =7.1%	

Table 5.16.2 Reaction rates of the $^{209}Bi(n,7n)^{203}Bi$ reaction on the main bar for 12 GeV proton bombardment.

Distance (cm)	Reaction Rate (/target nucleus/proton)	δ_{sta}	δ_{tot}
1	2.30E-28	1.5%	5.3%
5	2.99E-28	1.2%	7.2%
9	3.70E-28	1.1%	7.2%
17	5.04E-28	1.0%	7.2%
27	4.32E-28	1.2%	7.2%
55	1.77E-28	1.8%	7.3%
80	6.26E-29	3.4%	7.9%
100	2.68E-29	4.4%	8.4%
		δ_{sys} =7.1%	

Table 5.16.3 Reaction rates of the $^{209}Bi(n,7n)^{203}Bi$ reaction on the main bar for 24 GeV proton bombardment.

Distance (cm)	Reaction Rate (/target nucleus/proton)	δ_{sta}	δ_{tot}
1	3.42E-28	1.7%	7.3%
5	4.60E-28	1.4%	7.2%
9	6.12E-28	1.2%	7.2%
17	7.75E-28	1.1%	7.2%
27	7.72E-28	1.2%	7.2%
55	3.81E-28	1.6%	7.3%
80	1.38E-28	2.8%	7.7%
100	6.11E-29	4.3%	8.3%
		δ_{sys} =7.1%	

Table 6 List of the fitting parameters for the reaction rate data with the equation [a)]

Reaction	E_p(GeV)	Position	Region [b)]	a_1	a_2	a_3	a_4	a_5	a_6
$^{115}In(n,2n)^{115m}In$	1.94	Main	-1~100	2.56E-25	6.94E-02	-1.92E-25	7.10E-02	-6.31E-26	6.95E-02
		Sub-1	-1~85	3.50E-24	5.26E-02	-1.84E-24	5.36E-02	-1.67E-24	5.15E-02
		Sub-2	-1~85	4.01E-24	6.29E-02	-2.13E-24	6.40E-02	-1.88E-24	6.18E-02
		Sub-3	-1~100	2.58E-25	7.03E-02	-1.85E-25	7.20E-02	-7.11E-26	7.03E-02
	12	Main	-1~100	2.40E-23	4.29E-02	-1.25E-23	4.38E-02	-1.15E-23	4.21E-02
		Sub-1	-1~85	4.09E-24	3.12E-02	-2.20E-24	3.31E-02	-1.88E-24	2.92E-02
		Sub-2	-1~85	2.01E-23	3.70E-02	-1.05E-23	3.81E-02	-9.65E-24	3.60E-02
		Sub-3	-1~100	3.34E-23	4.77E-02	-1.74E-23	4.85E-02	-1.60E-23	4.68E-02
	24	Main	-1~100	3.66E-23	3.63E-02	-1.90E-23	3.72E-02	-1.75E-23	3.54E-02
		Sub-1	-1~85	1.37E-23	2.68E-02	-7.18E-24	2.82E-02	-6.46E-24	2.55E-02
		Sub-2	-1~85	3.67E-23	3.35E-02	-1.91E-23	3.45E-02	-1.76E-23	3.25E-02
		Sub-3	-1~100	5.15E-23	3.91E-02	-2.68E-23	4.00E-02	-2.47E-23	3.83E-02
$^{93}Nb(n,2n)^{92m}Nb$ [c)]	1.94	Main	1~100	2.48E-25	6.81E-02	-2.06E-25	6.81E-02	-4.20E-26	6.88E-02
	12	Main	1~100	3.38E-25	4.36E-02	-1.96E-25	4.59E-02	-1.41E-25	4.12E-02
	24	Main	1~100	3.04E-25	3.53E-02	-1.89E-25	3.81E-02	-1.14E-25	3.21E-02
$^{93}Nb(n,4n)^{90}Nb$ [c)]	1.94	Main	1~100	2.43E-25	6.40E-02	-2.14E-25	6.40E-02	-2.91E-26	6.45E-02
	12	Main	1~100	2.62E-25	4.01E-02	-1.99E-25	4.12E-02	-6.31E-26	3.73E-02
	24	Main	1~100	2.59E-25	3.49E-02	-2.02E-25	3.62E-02	-5.75E-26	3.13E-02
$^{27}Al(n,\alpha)^{24}Na$	1.94	Main	1~100	2.47E-25	7.05E-02	-2.09E-25	7.05E-02	-3.79E-26	7.05E-02
	12	Main	1~100	2.60E-25	4.49E-02	-2.00E-25	4.58E-02	-5.89E-26	4.23E-02
	24	Main	1~100	2.79E-25	3.76E-02	-1.89E-25	3.91E-02	-8.96E-26	3.52E-02
$^{59}Co(n,\alpha)^{56}Mn$	1.94	Main	1~100	2.42E-25	6.89E-02	-2.13E-25	6.90E-02	-2.93E-26	6.89E-02
	12	Main	1~100	2.39E-25	4.43E-02	-2.20E-25	4.46E-02	-1.94E-26	4.15E-02
	24	Main	1~100	2.45E-25	3.50E-02	-2.14E-25	3.54E-02	-3.12E-26	3.22E-02
$^{59}Co(n,2n)^{58}Co$	1.94	Main	1~100	2.55E-25	6.99E-02	-2.00E-25	7.02E-02	-5.37E-26	6.99E-02
	12	Main	1~100	6.28E-25	4.40E-02	-3.50E-25	4.63E-02	-2.76E-25	4.19E-02
	24	Main	1~100	1.02E-24	3.71E-02	-5.67E-25	3.93E-02	-4.54E-25	3.50E-02
$^{59}Co(n,3n)^{57}Co$	1.94	Main	1~100	2.40E-25	6.67E-02	-2.19E-25	6.68E-02	-2.17E-26	6.67E-02
	12	Main	1~100	2.63E-25	4.45E-02	-1.99E-25	4.56E-02	-6.36E-26	4.19E-02
	24	Main	1~100	3.02E-25	3.48E-02	-1.85E-25	3.67E-02	-1.17E-25	3.25E-02
$^{59}Co(n,4n)^{56}Co$	1.94	Main	1~100	2.35E-25	6.39E-02	-2.25E-25	6.39E-02	-1.01E-26	6.38E-02
	12	Main	1~100	2.35E-25	3.69E-02	-2.25E-25	3.70E-02	-9.60E-27	3.37E-02
	24	Main	1~100	2.37E-25	4.06E-02	-2.23E-25	4.09E-02	-1.47E-26	3.76E-02
$^{59}Co(n,5n)^{55}Co$	1.94	Main	1~100	2.30E-25	4.10E-02	-2.30E-25	4.10E-02	-6.69E-29	3.31E-02
	12	Main	1~100	2.30E-25	4.08E-02	-2.30E-25	4.09E-02	-2.50E-28	3.61E-02
	24	Main	1~100	2.30E-25	2.49E-02	-2.30E-25	2.49E-02	-9.11E-28	2.09E-02
$^{nat}Ni(n,x)^{58}Co$	1.94	Main	1~100	2.50E-25	6.94E-02	-2.06E-25	6.97E-02	-4.33E-26	6.95E-02
	12	Main	1~100	3.63E-25	4.30E-02	-2.09E-25	4.56E-02	-1.54E-25	4.05E-02
	24	Main	1~100	4.14E-25	3.73E-02	-2.39E-25	4.04E-02	-1.74E-25	3.44E-02
$^{nat}Ni(n,x)^{57}Co$	1.94	Main	1~100	2.50E-25	6.95E-02	-2.06E-25	6.97E-02	-4.33E-26	6.95E-02
	12	Main	1~100	3.63E-25	4.30E-02	-2.09E-25	4.56E-02	-1.54E-25	4.05E-02
	24	Main	1~100	4.14E-25	3.73E-02	-2.39E-25	4.04E-02	-1.74E-25	3.44E-02

a) $Y=a_1\exp(-a_2x)+a_3\exp(-a_4x)+a_5\exp(-a_6x)$, where Y is the reaction rate (per target nucleus and per incident proton), x is the distance between the top of the mercury target and the detector position in cm. and a_i (i=1~6) are the fitting parameters.

b) The region x where the experimental data exist.

c) The fitting is not done for the experimental data of the sub-bars, because the data are not so many to fit them with the 6-fitting-parameter-equation.

Table 6 (continued)

Reaction	E_p(GeV)	Position	Region[b)]	a_1	a_2	a_3	a_4	a_5	a_6
^{209}Bi(n,4n)^{206}Bi	1.94	Main	1~100	2.45E-25	7.15E-02	-2.14E-25	7.18E-02	-3.05E-26	7.14E-02
	12	Main	1~100	3.60E-25	4.27E-02	-2.07E-25	4.53E-02	-1.52E-25	4.02E-02
	24	Main	1~100	6.98E-25	3.65E-02	-3.88E-25	3.88E-02	-3.08E-25	3.44E-02
^{209}Bi(n,5n)^{205}Bi	1.94	Main	1~100	2.42E-25	6.43E-02	-2.17E-25	6.45E-02	-2.53E-26	6.43E-02
	12	Main	1~100	3.30E-25	4.25E-02	-1.94E-25	4.48E-02	-1.36E-25	4.01E-02
	24	Main	1~100	3.72E-25	3.41E-02	-2.13E-25	3.68E-02	-1.58E-25	3.15E-02
^{209}Bi(n,6n)^{204}Bi	1.94	Main	1~100	2.44E-25	6.67E-02	-2.13E-25	6.68E-02	-3.06E-26	6.67E-02
	12	Main	1~100	2.82E-25	4.16E-02	-1.88E-25	4.32E-02	-9.30E-26	3.91E-02
	24	Main	1~100	2.63E-25	3.55E-02	-1.99E-25	3.72E-02	-6.34E-26	3.17E-02
^{209}Bi(n,7n)^{203}Bi	1.94	Main	1~100	2.40E-25	6.54E-02	-2.20E-25	6.55E-02	-2.00E-26	6.56E-02
	12	Main	1~100	2.55E-25	4.31E-02	-2.06E-25	4.41E-02	-4.85E-26	4.02E-02
	24	Main	1~100	2.75E-25	3.56E-02	-1.92E-25	3.71E-02	-8.29E-26	3.29E-02

a) $RR=a_1\exp(-a_2x)+a_3\exp(-a_4x)+a_5\exp(-a_6x)$, where RR is the reaction rate (per target nucleus and per incident proton), x is the distance between the top of the mercury target and the detector position in cm. and a_i (i=1~6) are the fitting parameters.

b) The region x where the experimental data exist.

c) The fitting is not done for the experimental data of the sub-bars, because the data are not so many to fit them with the 6-fitting-parameter-equation.

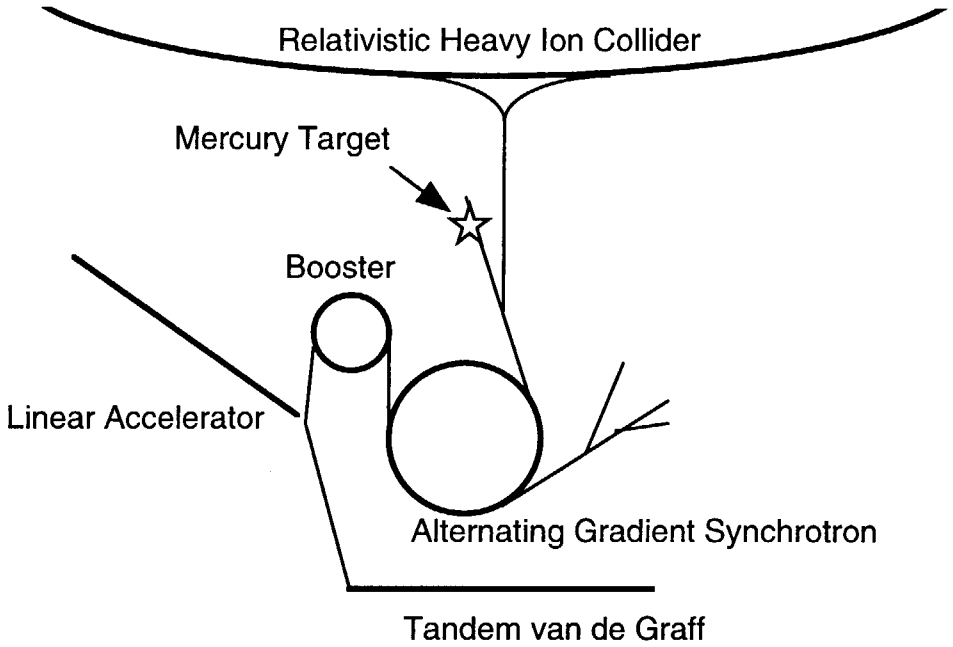

Fig.1 A plain view of the accelerator complex of Brookhaven National Laboratory. The mercury target was set in the U-line tunnel between AGS and Relativistic Heavy Ion Collider (RHIC).

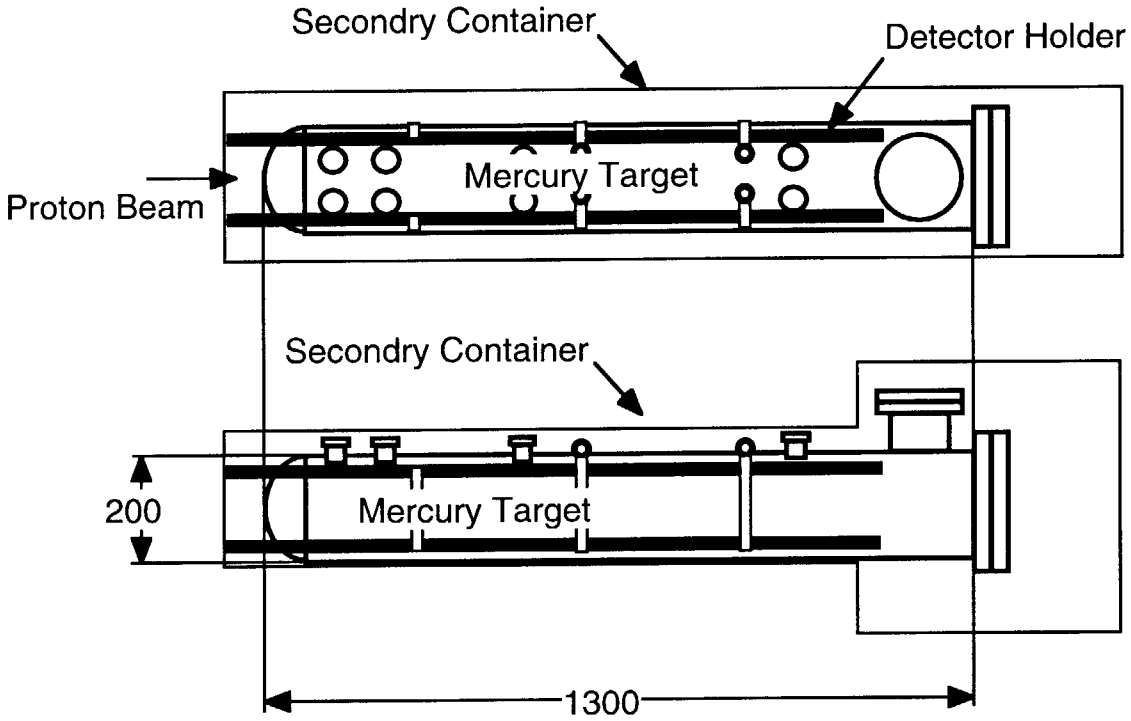

Fig. 2 Upper and side view of the mercury target. The unit of the values in the figure is in mm.

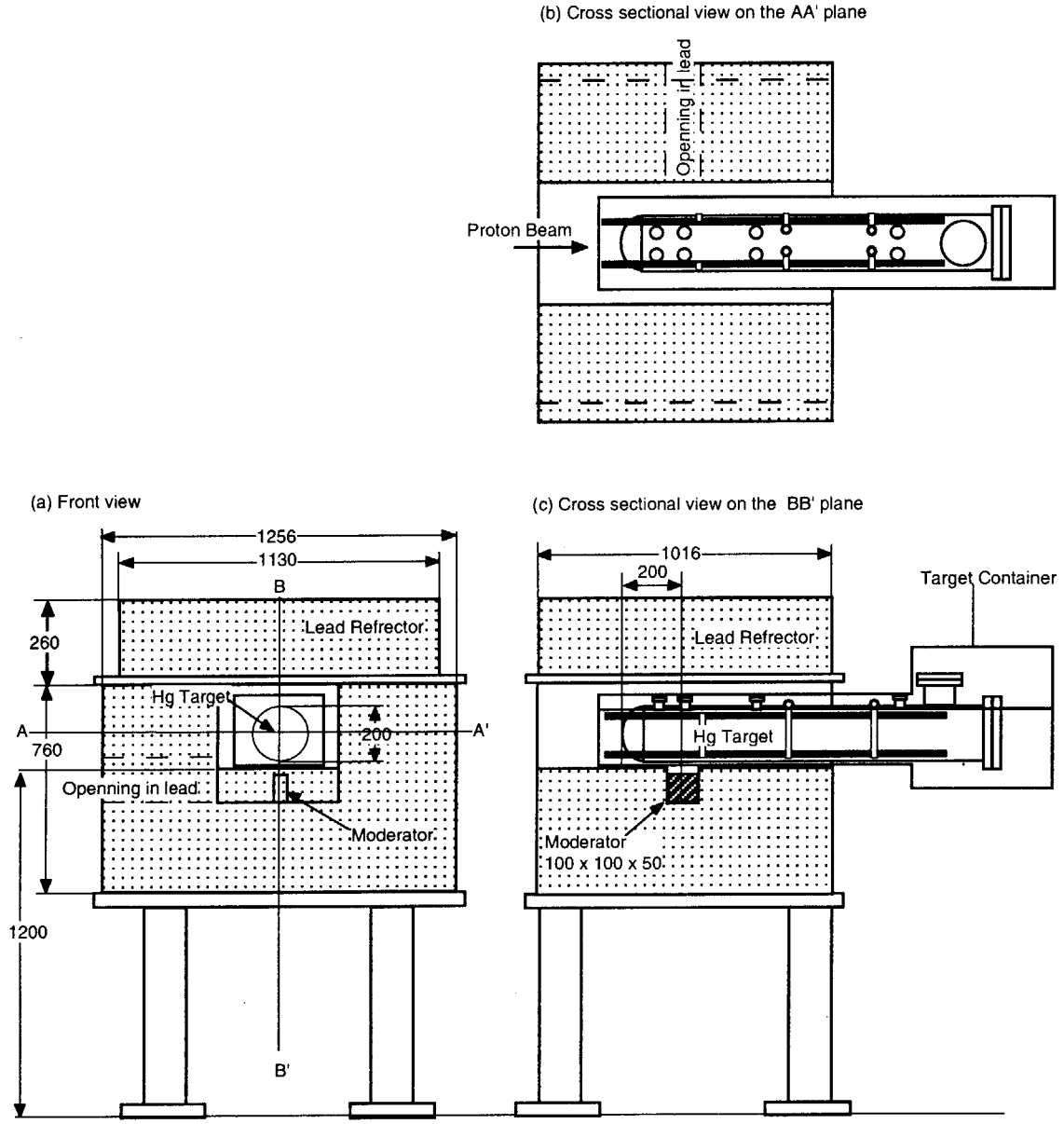

Fig. 3 Reflector and moderator: (a) front view, (b) cross sectional on BB' and (c) cross sectional view on AA'. The relative position of the mercury target for the reflector and the moderator could be changed by moving the mercury target. In the irradiation of activation detectors, the distance between the top of the mercury target and the center of the moderator was fixed on 200 mm.

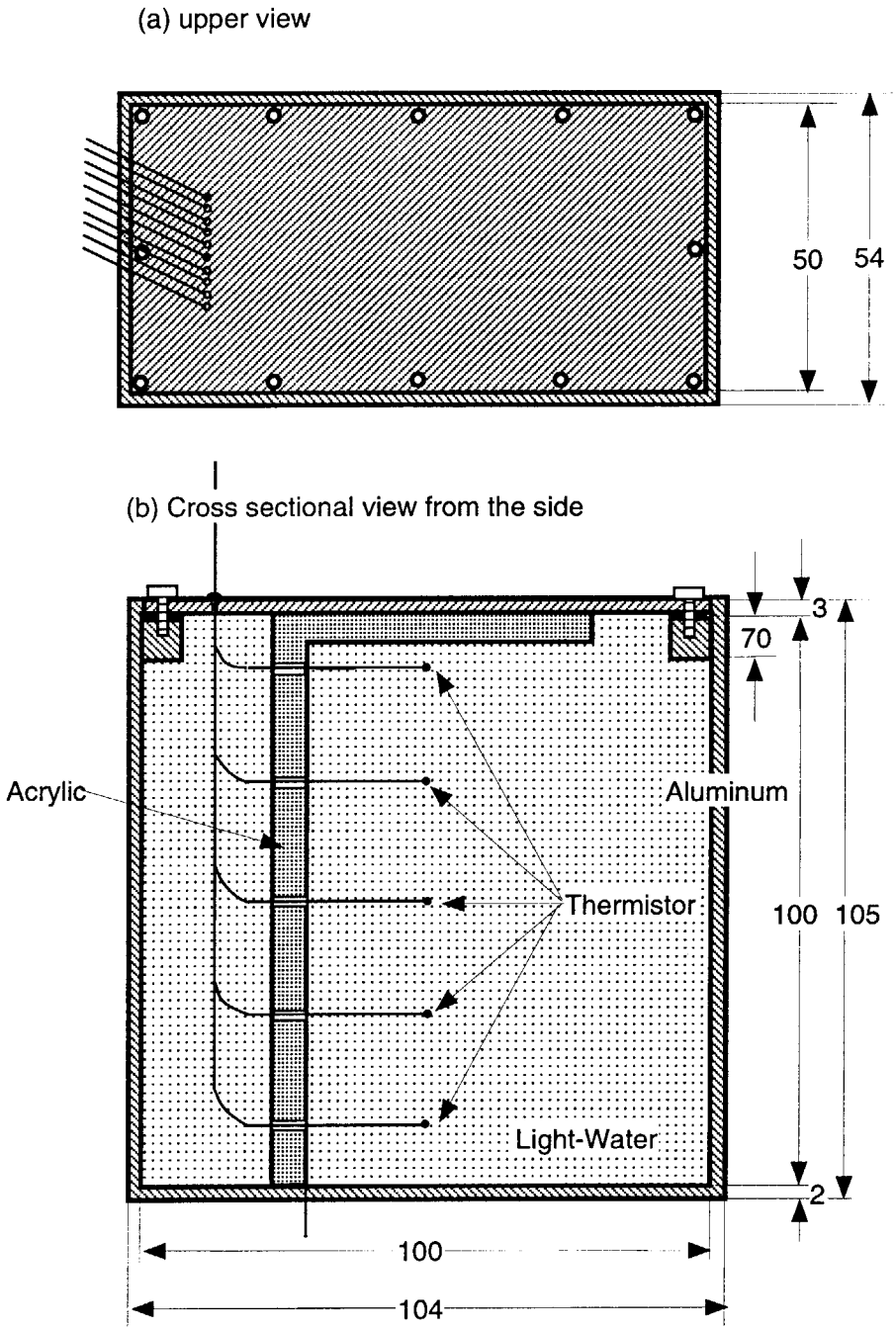

Fig. 4 Front and cross sectional view of the moderator. The box was made of aluminum with 2 mm in thickness. The inner size of the box was 100 mm × 100 mm × 50 mm. Five thermistors were set in the water to measure temperature rise of water by nuclear heating. The thermistors were fixed by the acrylic supporter.

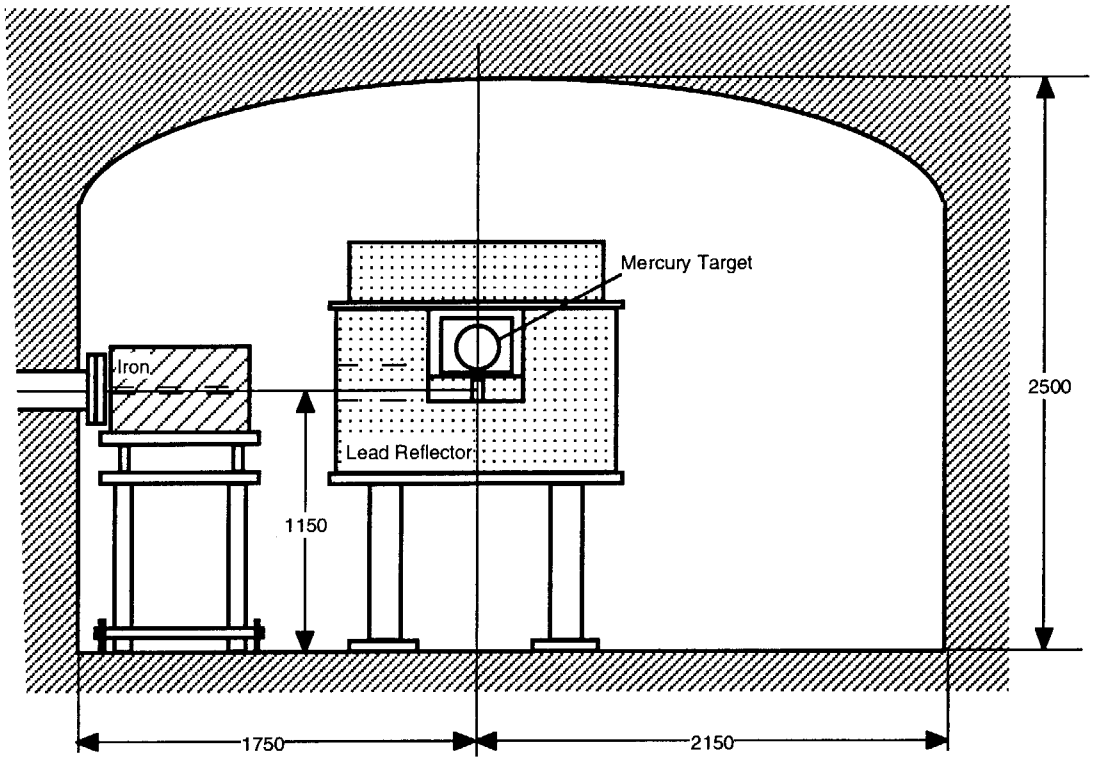

Fig. 5 Cross sectional view of the U-line block house in the AGS facility. The nominal proton beam height is 1250 mm. The center of the mercury target was placed at the beam axis. An iron with a slit was equipped besides the reflector for the TOF measurement. The unit of the value in the figure is in mm.

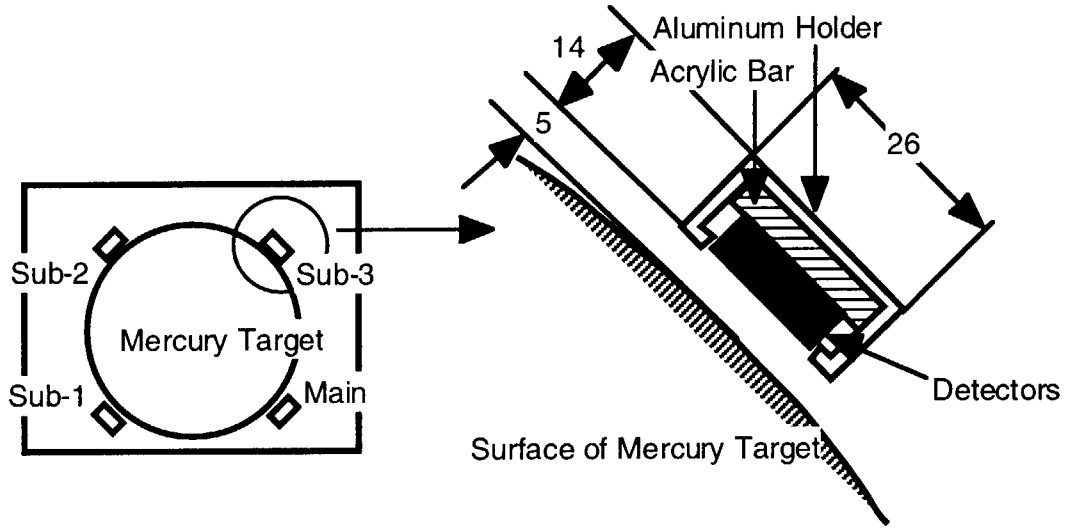

Fig. 6 Arrangement of activation-detector-holders (left) and configuration of the holder, an acrylic bar and a bundle of activation-detectors (right). The incident protons penetrate from the front to back surface. Four aluminum holders were set on surface of the mercury target. The activation detectors were put on the acrylic bars, and each bar were installed into the aluminum holders.

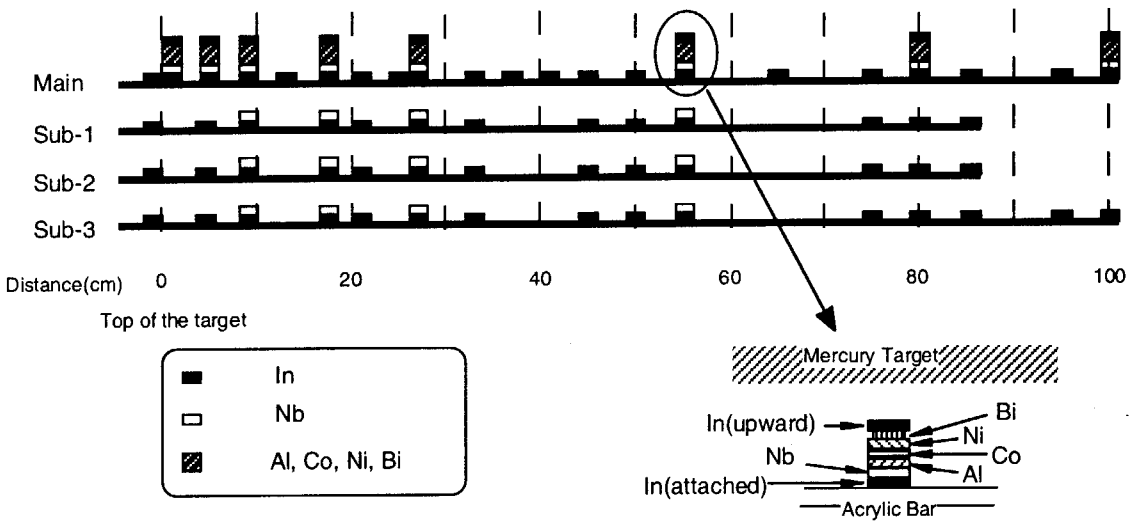

Fig. 7 Activation foils arrangement on the acrylic bar. Nickel, cobalt, aluminum and niobium foils were assembled in one foil stack. The stack was sandwiched with indium foils. The position of the indium foils were indicated as "upper" or "attached" as shown in the figure.

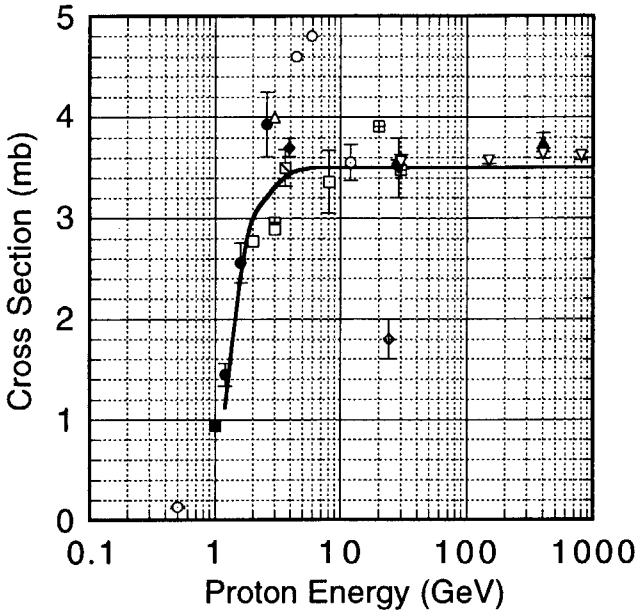

Fig. 8 Experimental cross section data for $Cu(p,x)^{24}Na$ reaction. The cross section values used to deduce the number of incident protons are 3.0, 3.5 and 3.5 mb for 1.94, 12 and 24 GeV, respectively. These cross section values were taken from the eye-guide line drawn in the figure.

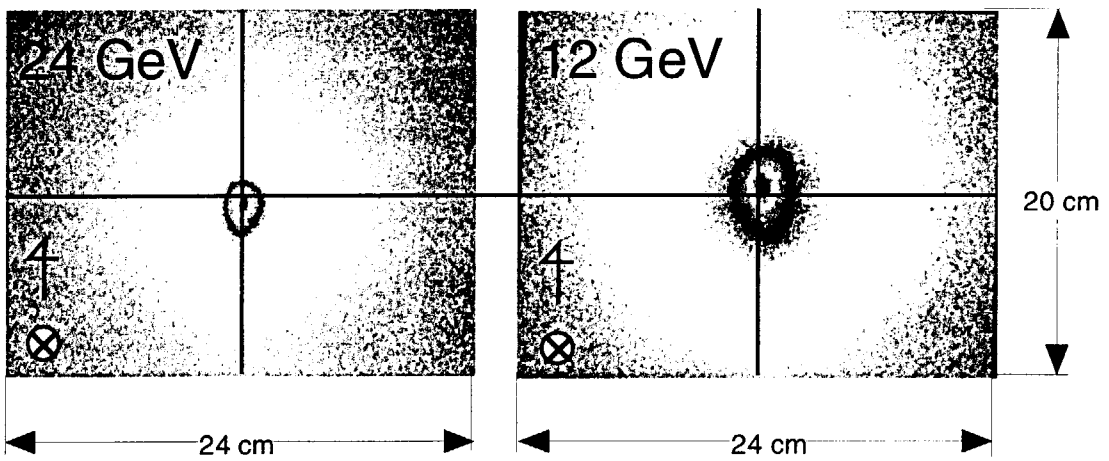

Fig. 9 Two-dimensional distribution of the incident protons for 24 and 12 GeV by imaging plate technique. The incident protons penetrate from the front to back surface. For 1.94 GeV proton bombardment, no obvious peak was observed in the image.

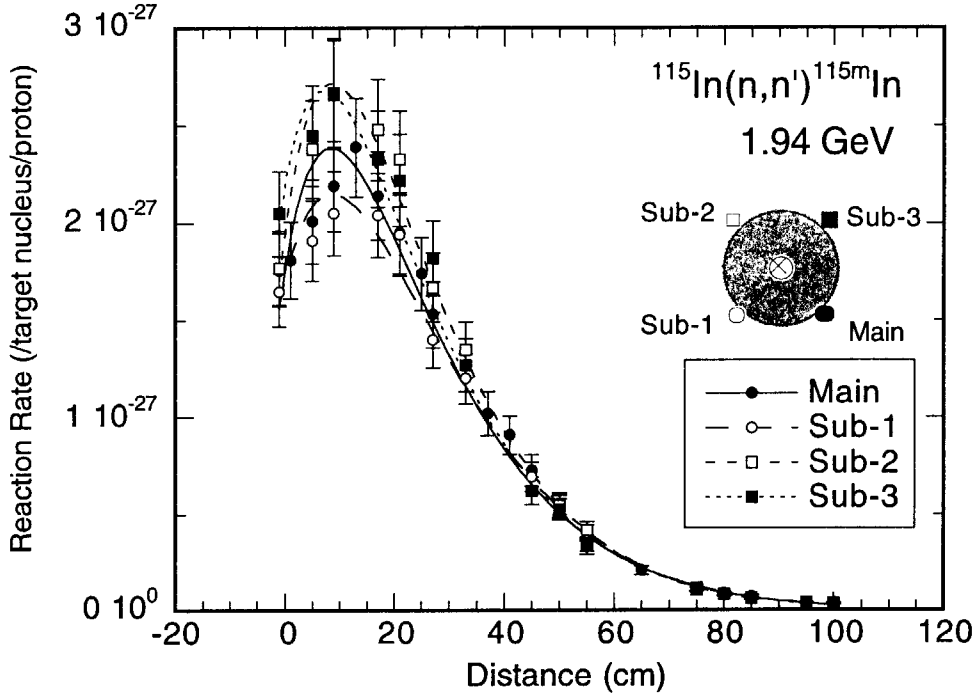

Fig. 10.1.1 Reaction rate distribution of the $^{115}In(n,n')^{115m}In$ reaction for 1.94 GeV protons. The lines show the fitting results with the function of eq.(3.1).

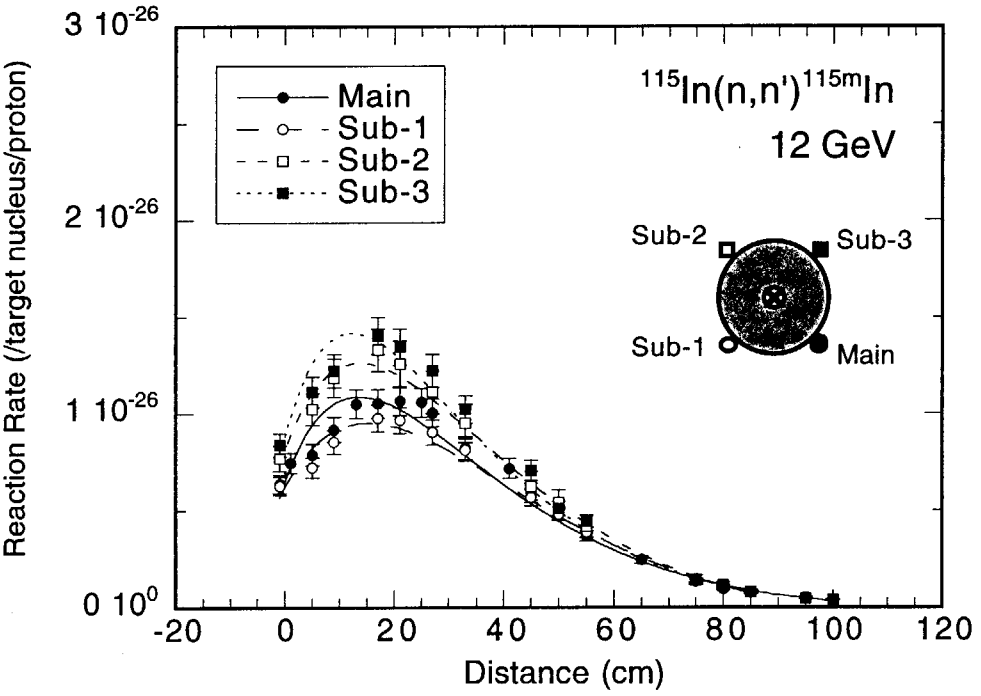

Fig. 10.1.2 Reaction rate distribution of the $^{115}In(n,n')^{115m}In$ reaction for 12 GeV protons. The lines show the fitting results with the function of eq. (3.1).

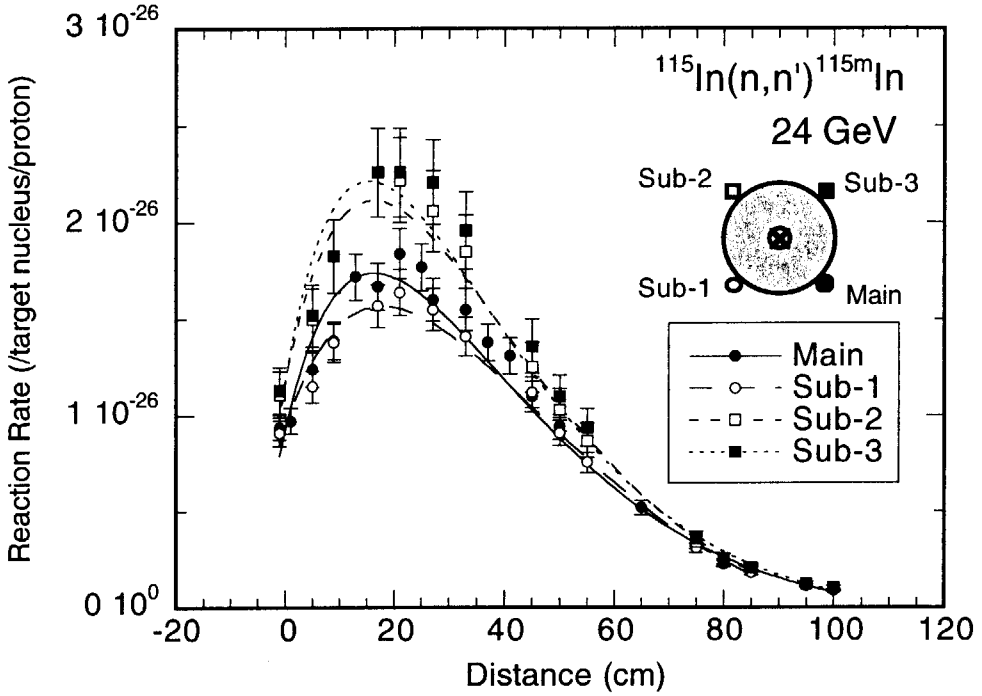

Fig. 10.1.3 Reaction rate distribution of the ^{115}In(n,n')^{115m}In reaction for 24 GeV protons. The lines show the fitting results with the function of eq. (3.1).

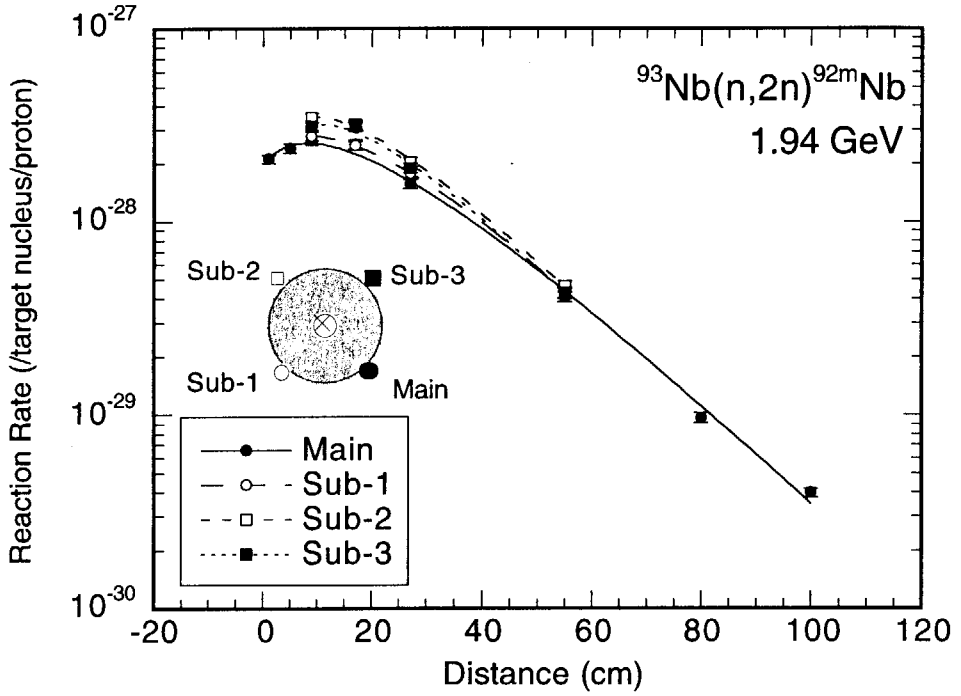

Fig. 10.2.1 Reaction rate distribution of the ^{93}Nb(n,2n')^{92m}Nb reaction for 1.94 GeV protons. The lines show the fitting results with the function of eq. (3.1).

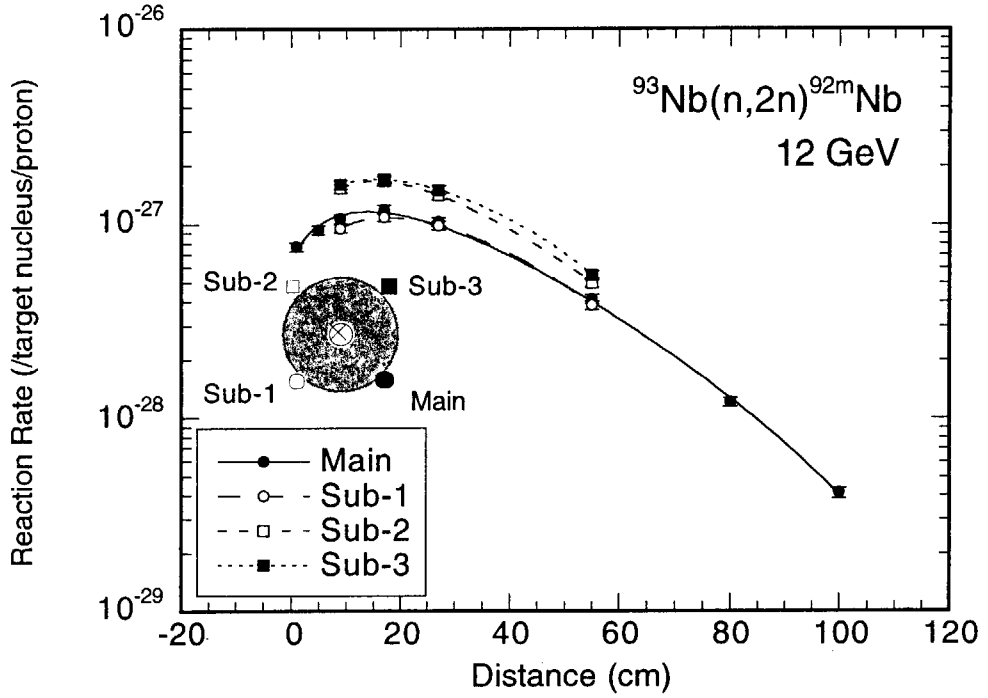

Fig. 10.2.2 Reaction rate distribution of the ^{93}Nb(n,2n')^{92m}Nb reaction for 12 GeV protons. The lines show the fitting results with the function of eq. (3.1).

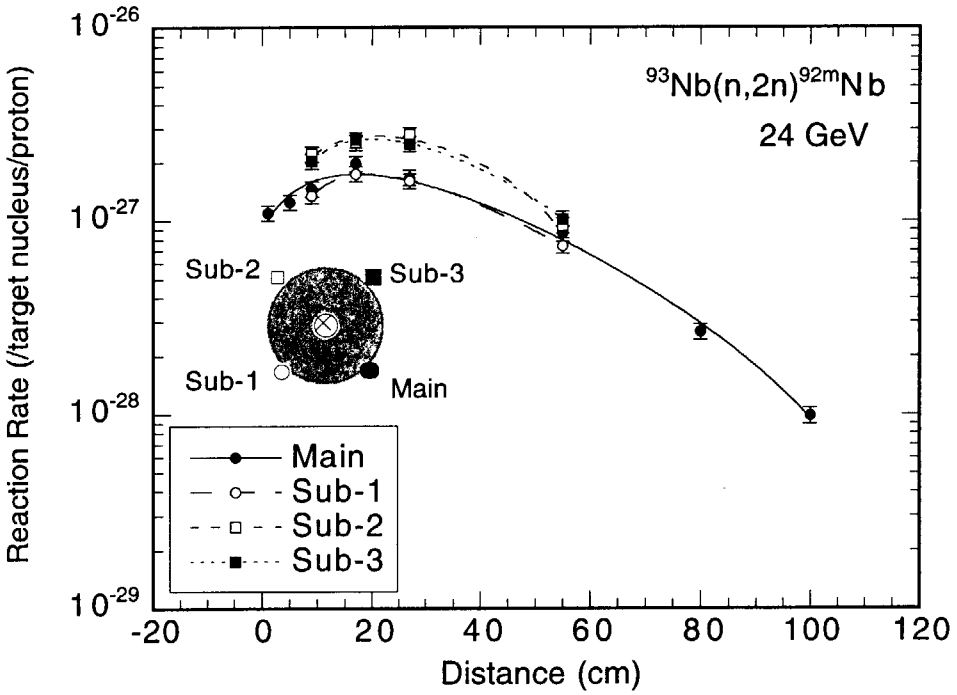

Fig. 10.2.3 Reaction rate distribution of the ^{93}Nb(n,2n')^{92m}Nb reaction for 24 GeV protons. The lines show the fitting results with the function of eq. (3.1).

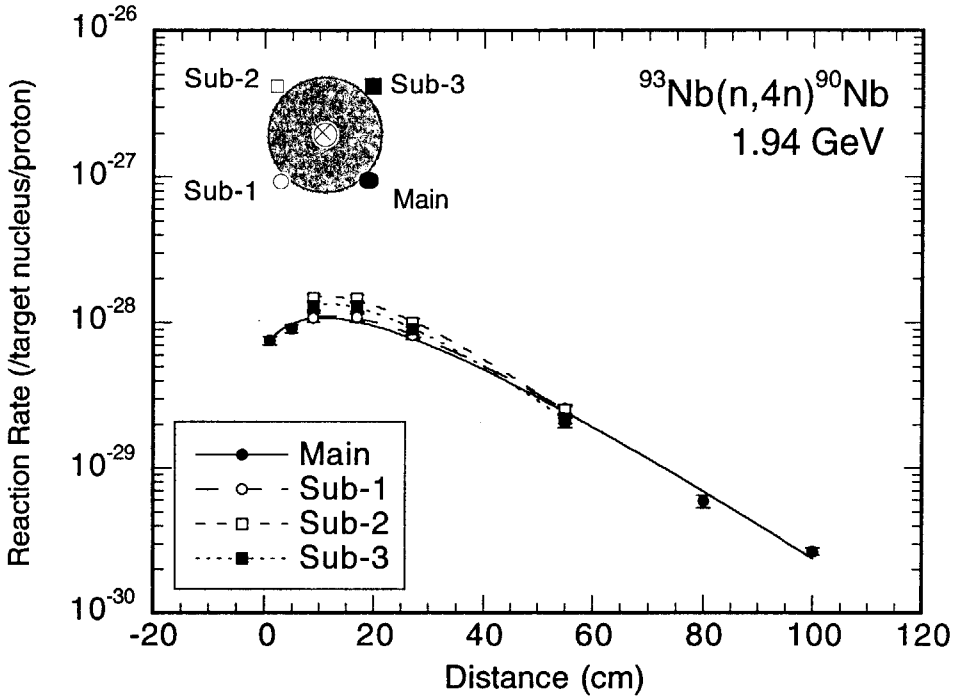

Fig. 10.3.1 Reaction rate distribution of the ^{93}Nb(n,4n')^{92m}Nb reaction for 1.94 GeV protons. The lines show the fitting results with the function of eq. (3.1).

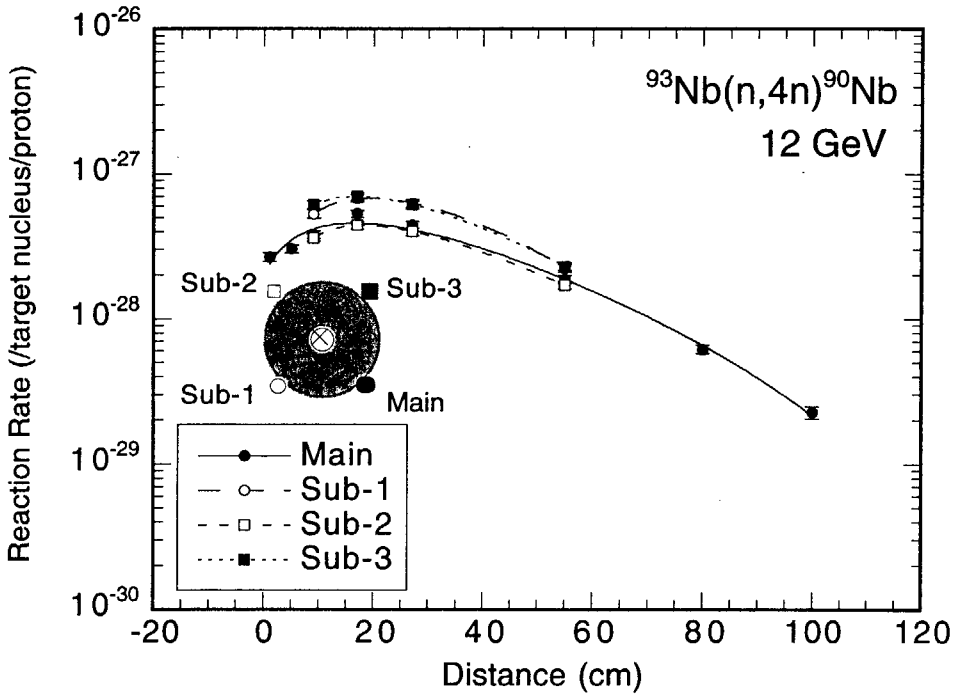

Fig. 10.3.2 Reaction rate distribution of the ^{93}Nb(n,4n')^{92m}Nb reaction for 12 GeV protons. The lines show the fitting results with the function of eq. (3.1).

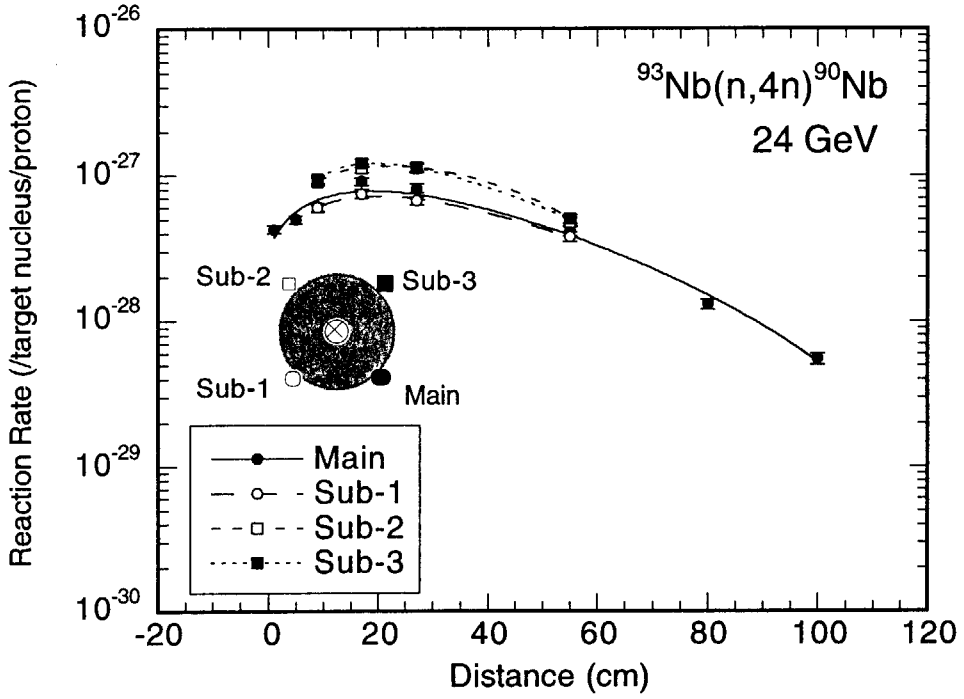

Fig. 10.3.3 Reaction rate distribution of the ^{93}Nb(n,4n')^{92m}Nb reaction for 24 GeV protons. The lines show the fitting results with the function of eq. (3.1).

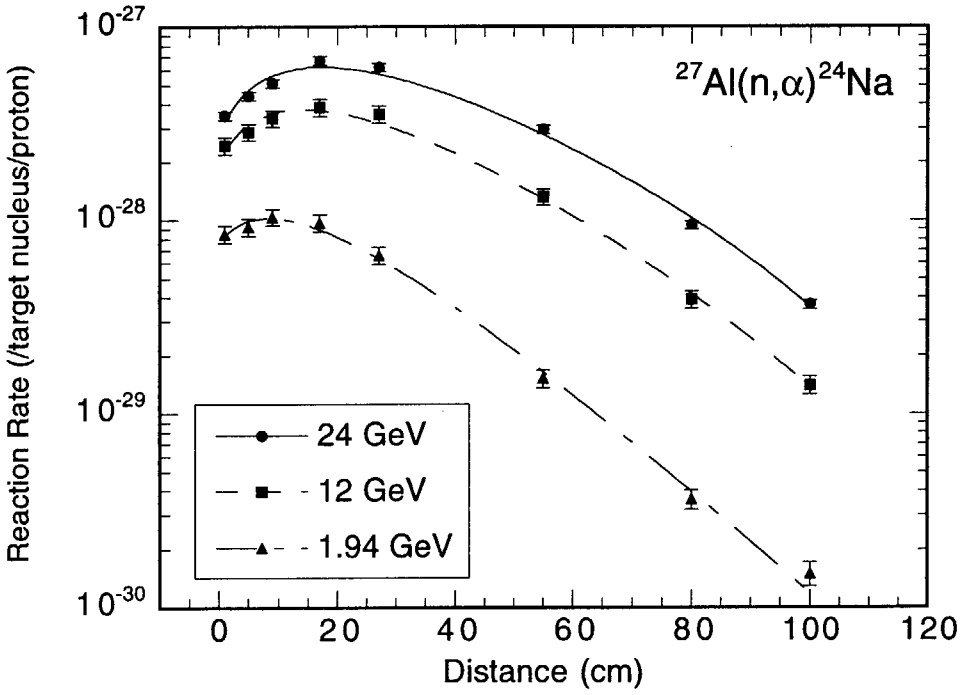

Fig. 10.4 Reaction rate distribution of the ^{27}Al(n,α)^{24}Na reaction for 1.94, 12 and 24 GeV protons. The lines show the fitting results with the function of eq. (3.1).

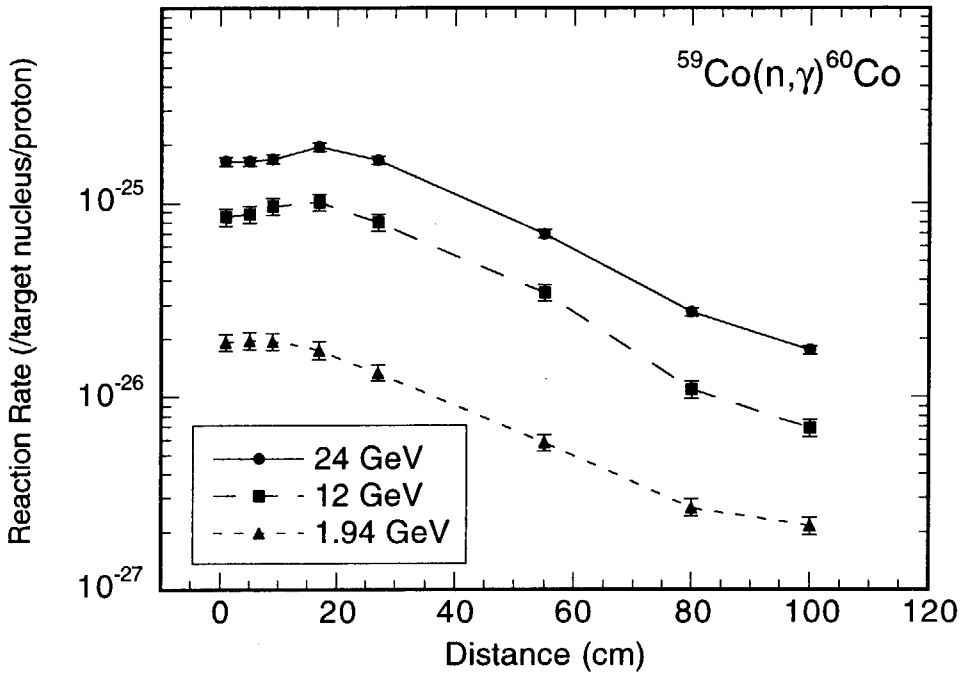

Fig. 10.5 Reaction rate distribution of the ^{59}Co(n,γ)^{60}Co reaction for 1.94, 12 and 24 GeV protons.

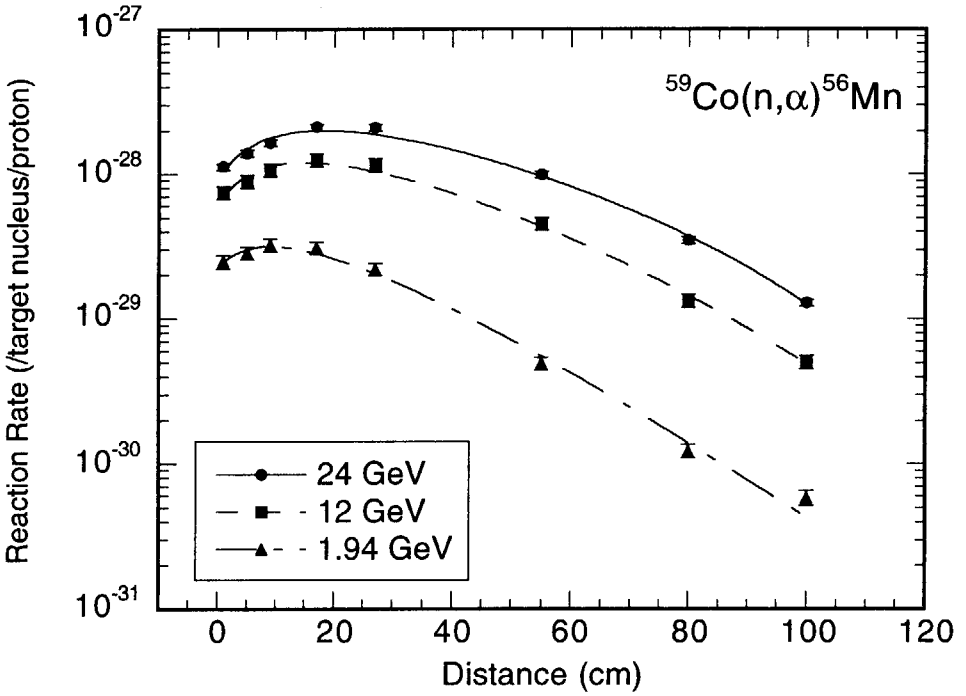

Fig. 10.6 Reaction rate distribution of the ^{59}Co(n,α)^{56}Mn reaction for 1.94, 12 and 24 GeV protons. The lines show the results with the function of eq. (3.1).

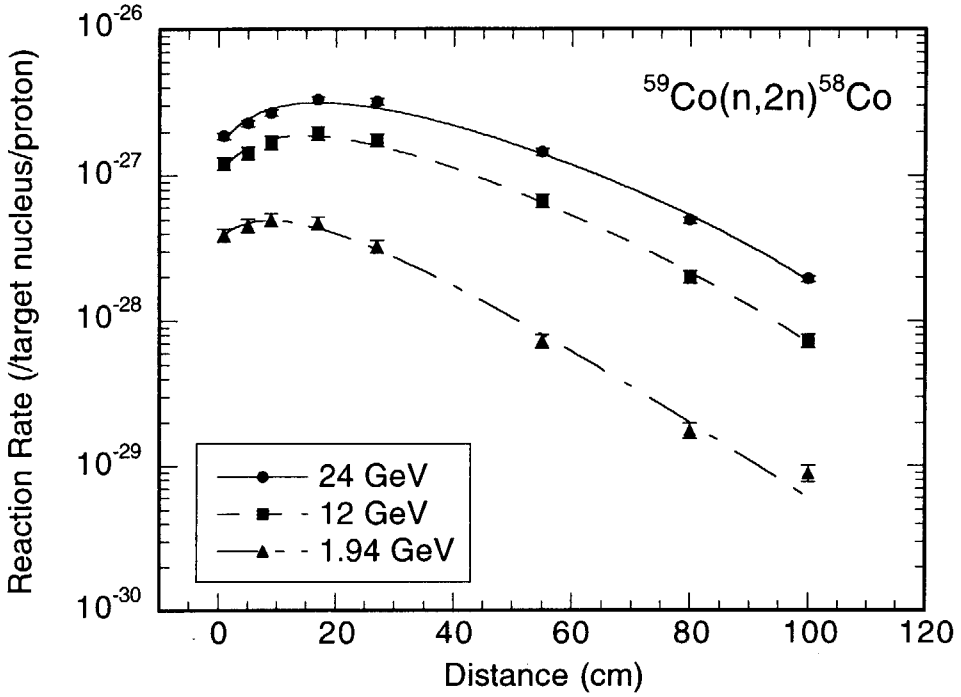

Fig. 10.7 Reaction rate distribution of the ^{59}Co(n,2n)^{58}Co reaction for 1.94, 12 and 24 GeV protons. The lines show the results with the function of eq. (3.1).

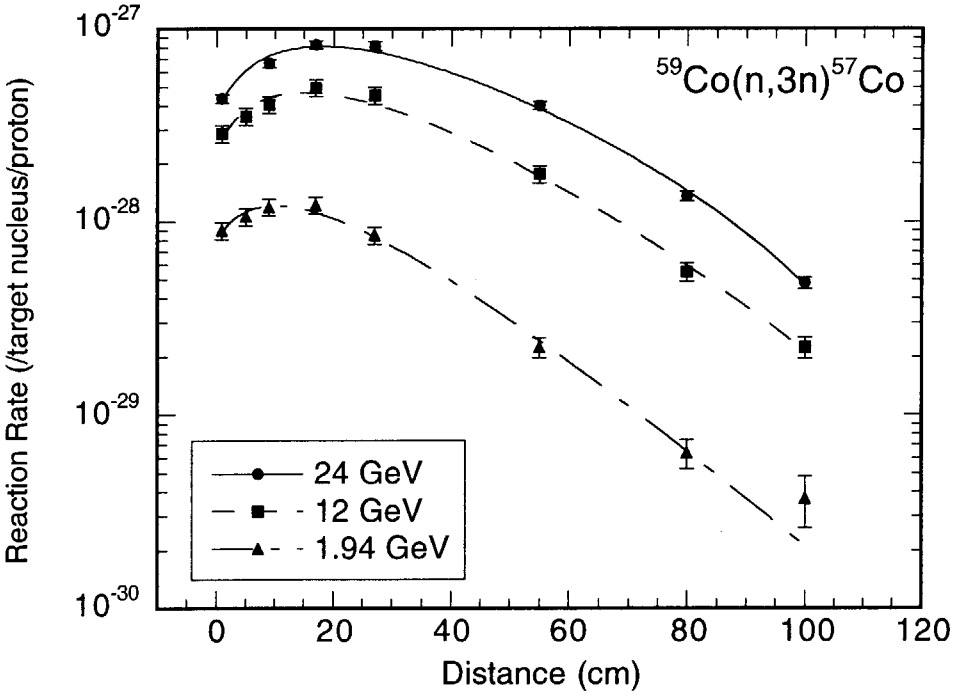

Fig. 10.8 Reaction rate distribution of the ^{59}Co(n,3n)^{57}Co reaction for 1.94, 12 and 24 GeV protons. The lines show the results with the function of eq. (3.1).

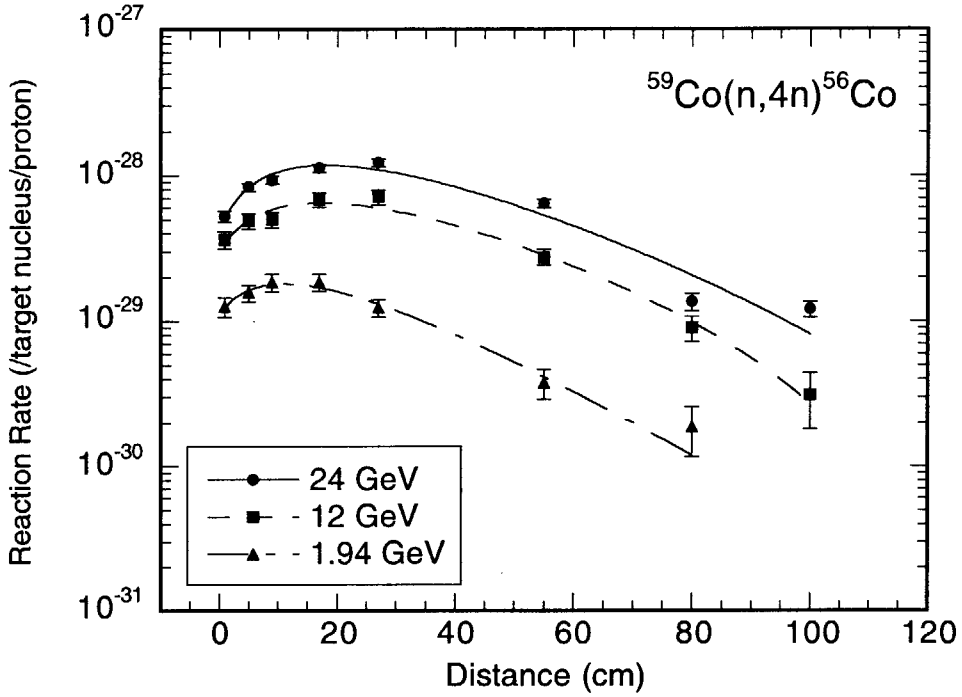

Fig. 10.9 Reaction rate distribution of the ^{59}Co(n,4n)^{56}Co reaction for 1.94, 12 and 24 GeV protons. The lines show the results with the function of eq. (3.1).

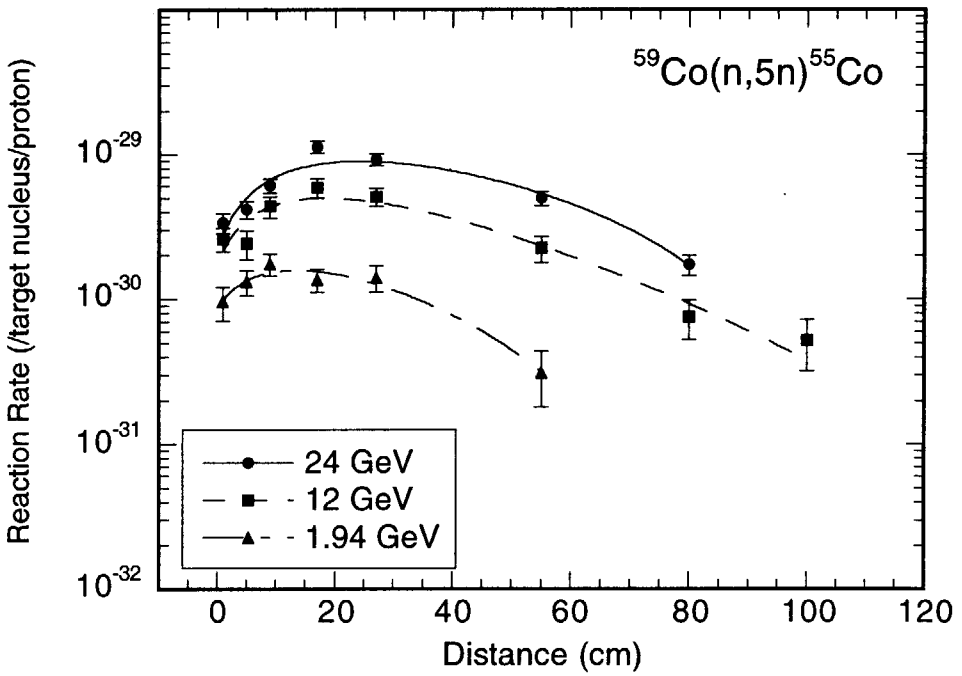

Fig. 10.10 Reaction rate distribution of the ^{59}Co(n,5n)^{55}Co reaction for 1.94, 12 and 24 GeV protons. The lines show the results with the function of eq. (3.1).

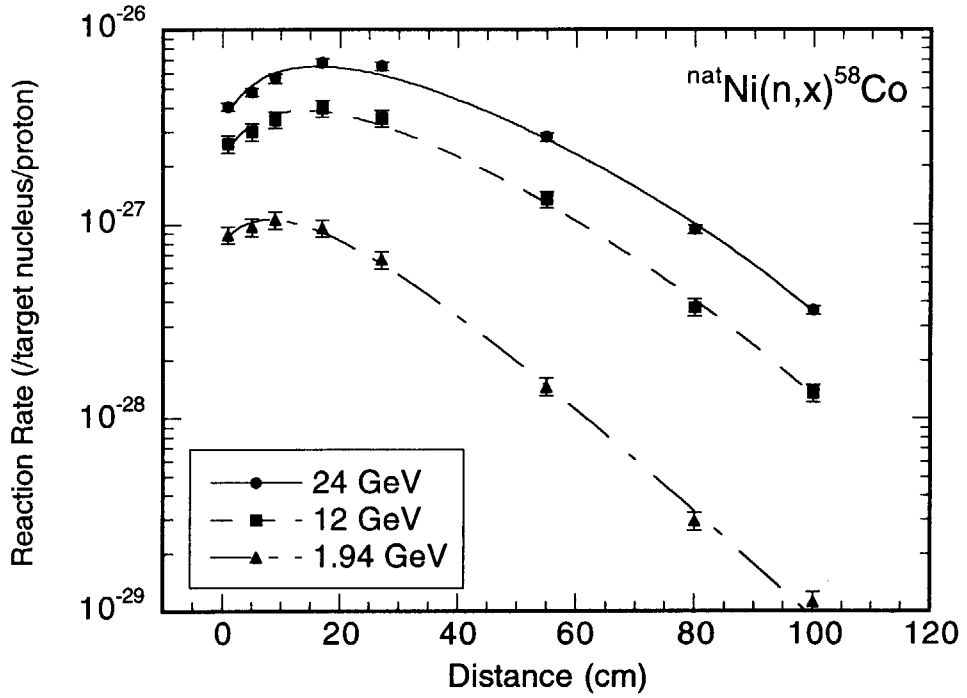

Fig. 10.11 Reaction rate distribution of the ^{nat}Ni(n,x)^{58}Co reaction for 1.94, 12 and 24 GeV protons. The lines show the results with the function of eq. (3.1).

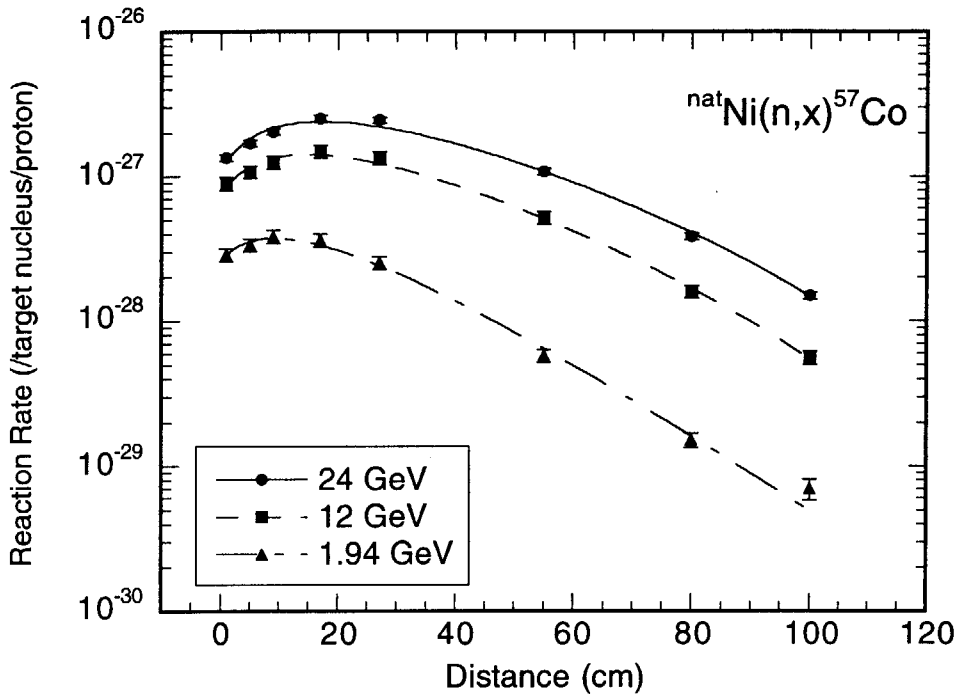

Fig. 10.12 Reaction rate distribution of the ^{nat}Ni(n,x)^{57}Co reaction for 1.94, 12 and 24 GeV protons. The lines show the results with the function of eq. (3.1).

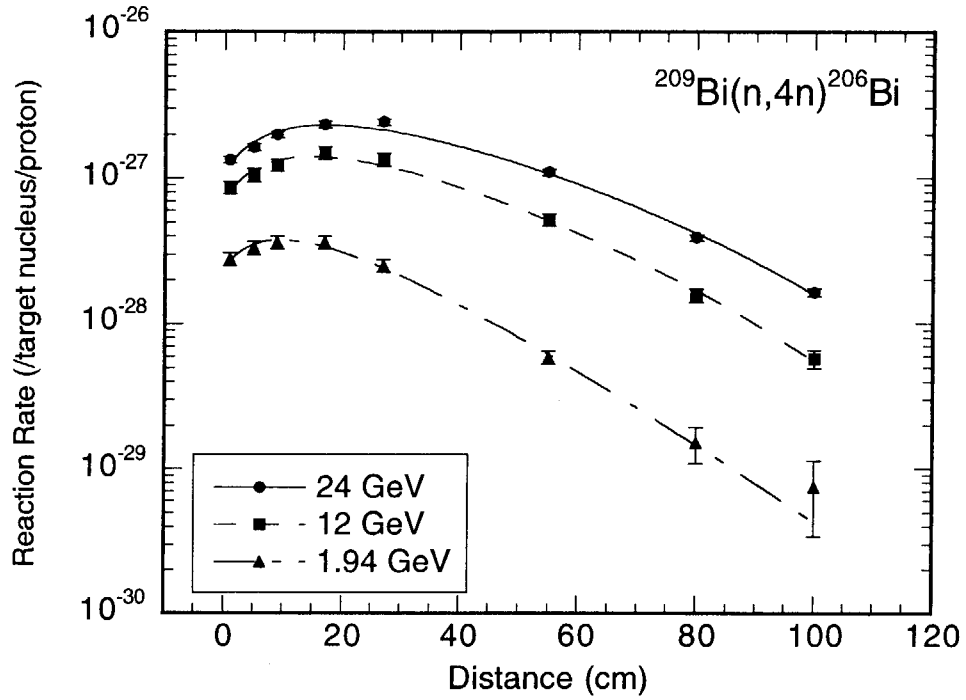

Fig. 10.13 Reaction rate distribution of the ^{209}Bi(n,4n)^{206}Bi reaction for 1.94, 12 and 24 GeV protons. The lines show the results with the function of eq. (3.1).

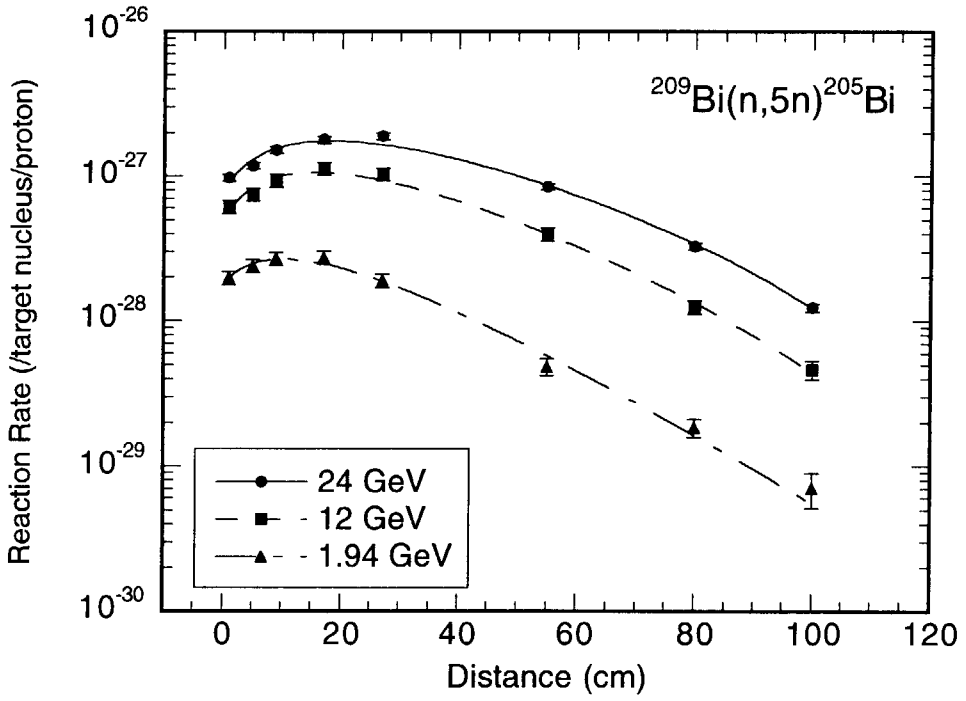

Fig. 10.14 Reaction rate distribution of the ^{209}Bi(n,5n)^{205}Bi reaction for 1.94, 12 and 24 GeV protons. The lines show the results with the function of eq. (3.1).

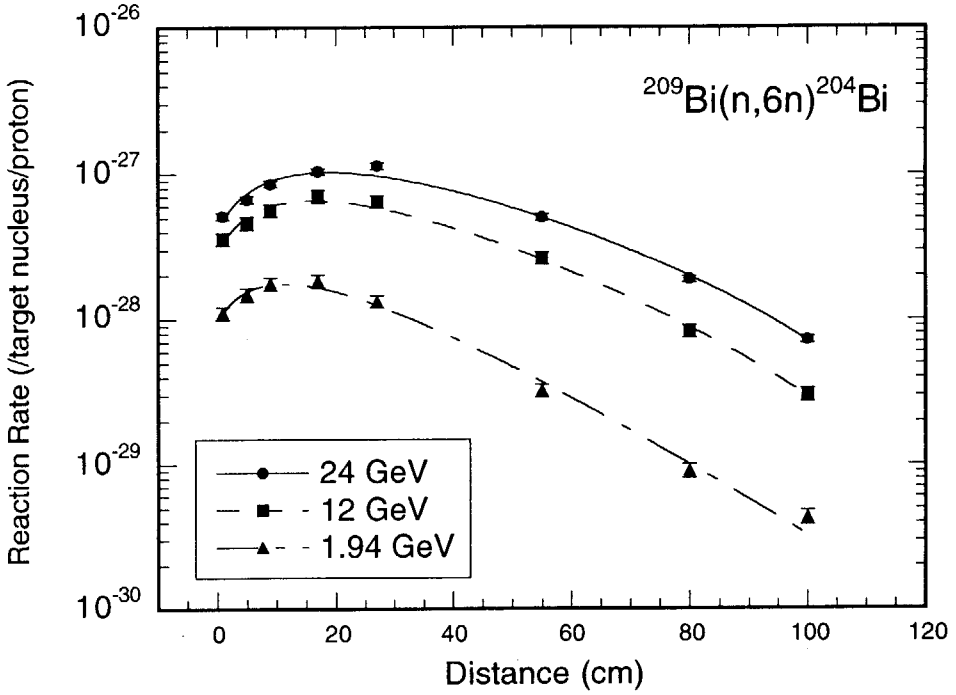

Fig. 10.14 Reaction rate distribution of the ^{209}Bi(n,6n)^{204}Bi reaction for 1.94, 12 and 24 GeV protons. The lines show the results with the function of eq. (3.1).

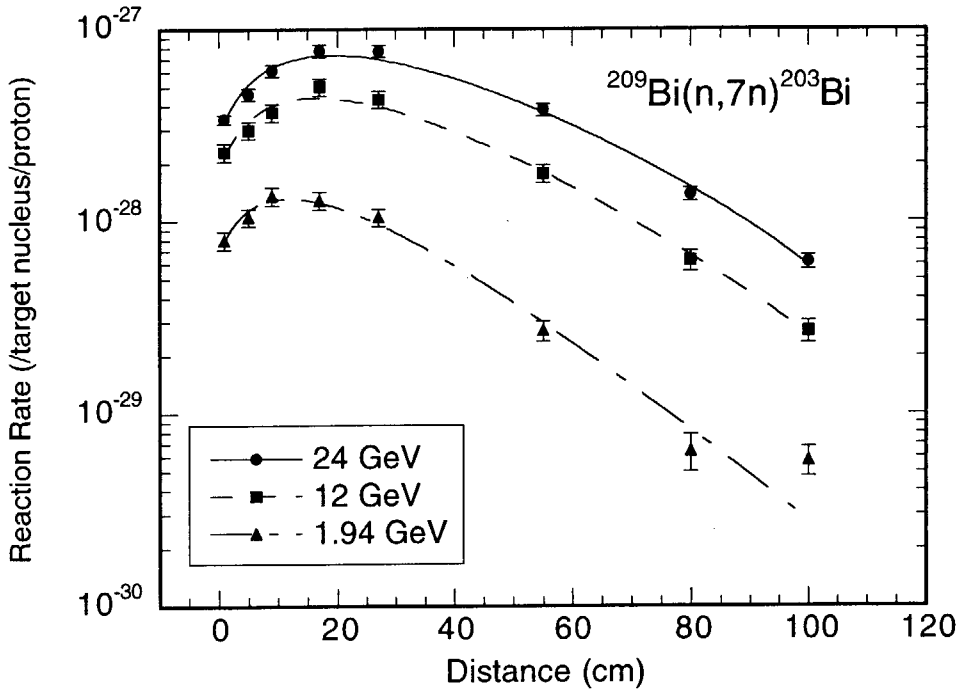

Fig. 10.15 Reaction rate distribution of the ^{209}Bi(n,7n)^{203}Bi reaction for 1.94, 12 and 24 GeV protons. The lines show the results with the function of eq. (3.1).

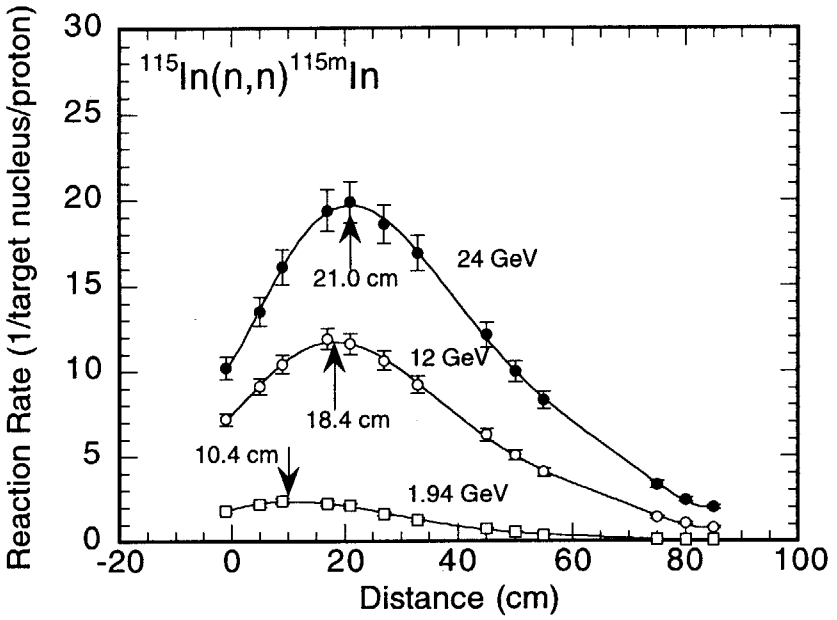

Fig. 11.1 Averaged reaction rates of the $^{115}In(n,n')^{115m}In$ reaction. The peak positions of the reaction rate distributions are indicated by the arrows, and the distance from the top of the target is shown. The peak position of the reaction rates moves to deeper position with increase of the incident proton energy.

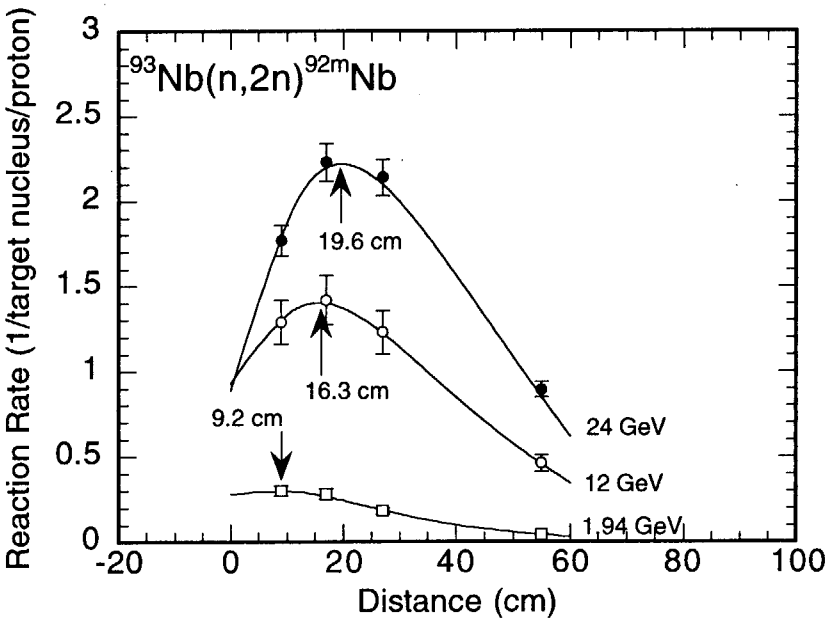

Fig. 11.2 Averaged reaction rates of the $^{93}Nb(n,2n)^{92m}Nb$ reaction. The peak positions of the reaction rate distributions are indicated by the arrows, and the distance from the top of the target is shown. The peak position of the reaction rates moves to deeper position with increase of the incident proton energy.

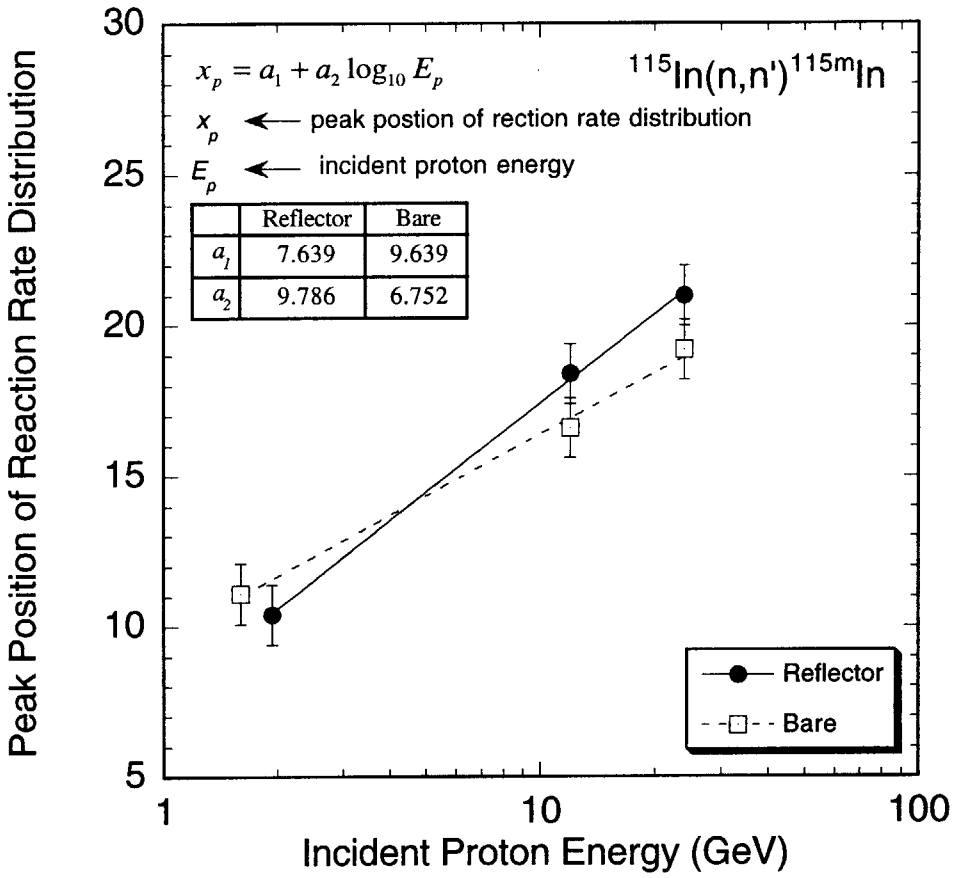

Fig. 12.1 Validation of peak position of the ^{115}In(n,n')^{115m}In reaction rates as a function of incident energy. The solid and dotted lines show the fitting results for the present target assembly and the bare target, respectively.

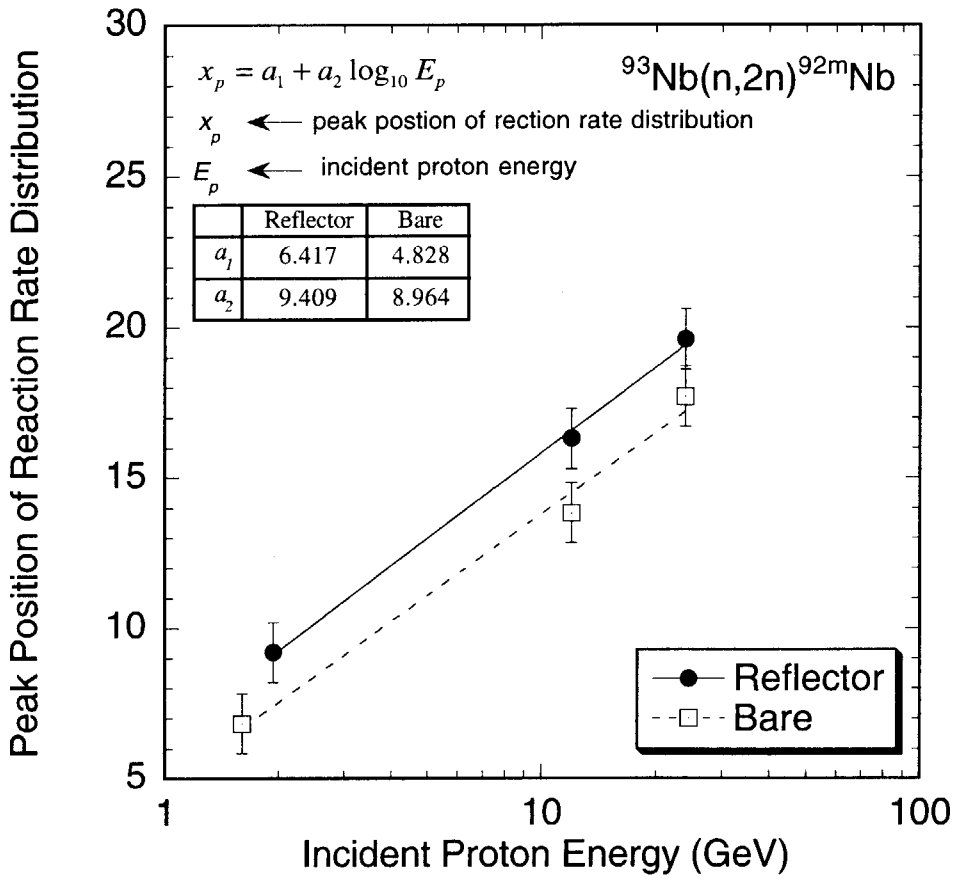

Fig. 12.2 Validation of peak position of the ^{93}Nb(n,2n)^{92m}Nb reaction rates as a function of incident energy. The solid and dotted lines show the fitting results for the present target assembly and the bare target, respectively.

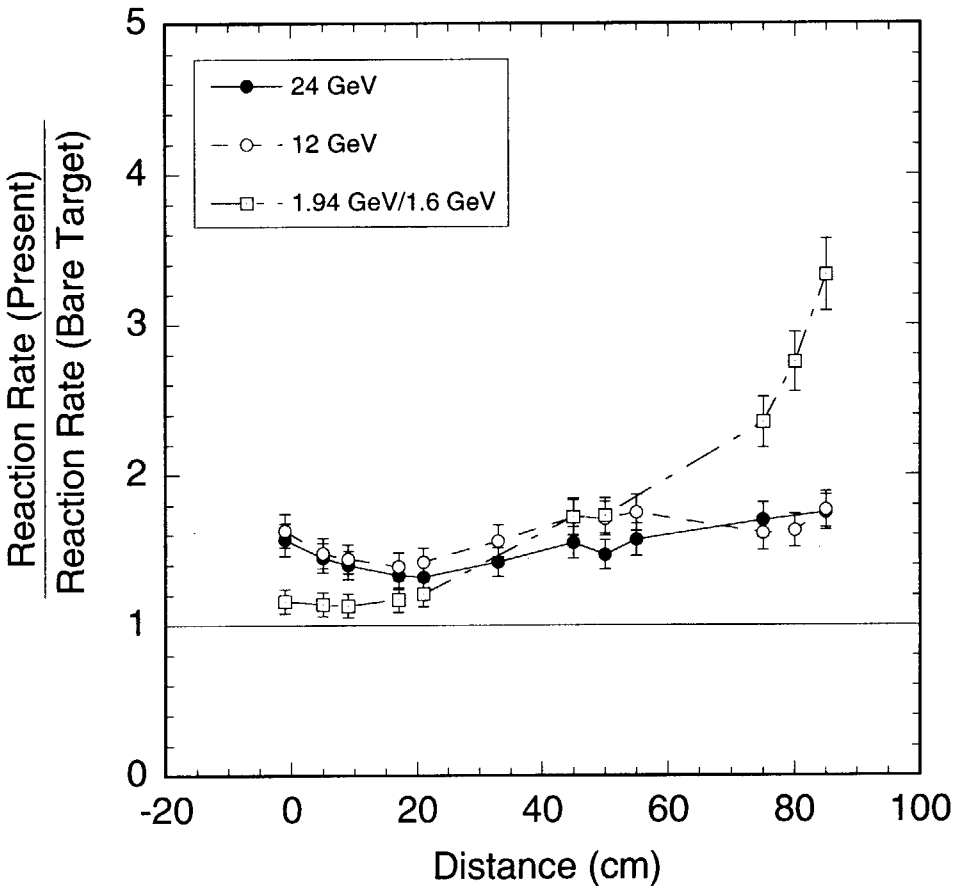

Fig. 13.1 Ratio of the reaction rates of the mercury target surrounded by the reflector to those of the bare target for the $^{115}In(n,n')^{115m}In$ reaction. The averaged reaction rates are used to deduce the ratios.

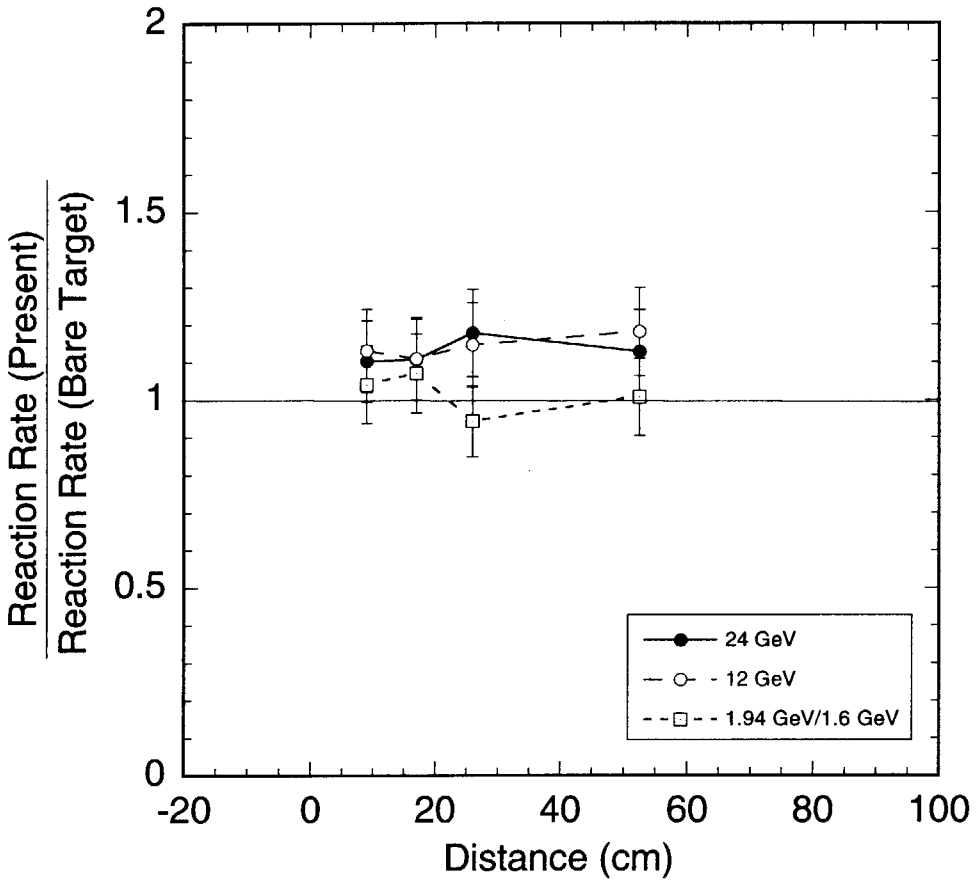

Fig. 13.2 Ratio of the reaction rates of the mercury target surrounded by the reflector to those of the bare target for the $^{93}Nb(n,2n)^{92m}Nb$ reaction. The averaged reaction rates are used to deduce the ratios.

国際単位系（SI）と換算表

表1　SI基本単位および補助単位

量	名称	記号
長さ	メートル	m
質量	キログラム	kg
時間	秒	s
電流	アンペア	A
熱力学温度	ケルビン	K
物質量	モル	mol
光度	カンデラ	cd
平面角	ラジアン	rad
立体角	ステラジアン	sr

表2　SIと併用される単位

名称	記号
分，時，日	min，h，d
度，分，秒	°，′，″
リットル	l，L
トン	t
電子ボルト	eV
原子質量単位	u

1 eV=1.60218×10^{-19}J

1 u=1.66054×10^{-27}kg

表3　固有の名称をもつSI組立単位

量	名称	記号	他のSI単位による表現
周波数	ヘルツ	Hz	s^{-1}
力	ニュートン	N	$m\cdot kg/s^2$
圧力，応力	パスカル	Pa	N/m^2
エネルギー,仕事,熱量	ジュール	J	N·m
工率，放射束	ワット	W	J/s
電気量，電荷	クーロン	C	A·s
電位，電圧，起電力	ボルト	V	W/A
静電容量	ファラド	F	C/V
電気抵抗	オーム	Ω	V/A
コンダクタンス	ジーメンス	S	A/V
磁束	ウェーバ	Wb	V·s
磁束密度	テスラ	T	Wb/m^2
インダクタンス	ヘンリー	H	Wb/A
セルシウス温度	セルシウス度	℃	
光束	ルーメン	lm	cd·sr
照度	ルクス	lx	lm/m^2
放射能	ベクレル	Bq	s^{-1}
吸収線量	グレイ	Gy	J/kg
線量等量	シーベルト	Sv	J/kg

表4　SIと共に暫定的に維持される単位

名称	記号
オングストローム	Å
バーン	b
バール	bar
ガル	Gal
キュリー	Ci
レントゲン	R
ラド	rad
レム	rem

1 Å=0.1nm=10^{-10}m

1 b=100fm^2=10^{-28}m^2

1 bar=0.1MPa=10^{5}Pa

1 Gal=1cm/s^2=10^{-2}m/s^2

1 Ci=3.7×10^{10}Bq

1 R=2.58×10^{-4}C/kg

1 rad=1cGy=10^{-2}Gy

1 rem=1cSv=10^{-2}Sv

表5　SI接頭語

倍数	接頭語	記号
10^{18}	エクサ	E
10^{15}	ペタ	P
10^{12}	テラ	T
10^{9}	ギガ	G
10^{6}	メガ	M
10^{3}	キロ	k
10^{2}	ヘクト	h
10^{1}	デカ	da
10^{-1}	デシ	d
10^{-2}	センチ	c
10^{-3}	ミリ	m
10^{-6}	マイクロ	μ
10^{-9}	ナノ	n
10^{-12}	ピコ	p
10^{-15}	フェムト	f
10^{-18}	アト	a

(注)

1．表1－5は「国際単位系」第5版，国際度量衡局1985年刊行による。ただし，1 eVおよび1 uの値はCODATAの1986年推奨値によった。

2．表4には海里，ノット，アール，ヘクタールも含まれているが日常の単位なのでここでは省略した。

3．barは，JISでは流体の圧力を表わす場合に限り表2のカテゴリーに分類されている。

4．EC閣僚理事会指令ではbar，barnおよび「血圧の単位」mmHgを表2のカテゴリーに入れている。

換算表

力	N(=10^{5}dyn)	kgf	lbf
	1	0.101972	0.224809
	9.80665	1	2.20462
	4.44822	0.453592	1

粘度　1 Pa·s(N·s/m^2)=10 P(ポアズ)(g/(cm·s))

動粘度　1m^2/s=10^{4}St(ストークス)(cm^2/s)

圧力	MPa(=10bar)	kgf/cm^2	atm	mmHg(Torr)	lbf/in^2(psi)
	1	10.1972	9.86923	7.50062×10^3	145.038
	0.0980665	1	0.967841	735.559	14.2233
	0.101325	1.03323	1	760	14.6959
	1.33322×10^{-4}	1.35951×10^{-3}	1.31579×10^{-3}	1	1.93368×10^{-2}
	6.89476×10^{-3}	7.03070×10^{-2}	6.80460×10^{-2}	51.7149	1

エネルギー・仕事・熱量	J(=10^7 erg)	kgf·m	kW·h	cal(計量法)	Btu	ft·lbf	eV
	1	0.101972	2.77778×10^{-7}	0.238889	9.47813×10^{-4}	0.737562	6.24150×10^{18}
	9.80665	1	2.72407×10^{-6}	2.34270	9.29487×10^{-3}	7.23301	6.12082×10^{19}
	3.6×10^6	3.67098×10^5	1	8.59999×10^5	3412.13	2.65522×10^6	2.24694×10^{25}
	4.18605	0.426858	1.16279×10^{-6}	1	3.96759×10^{-3}	3.08747	2.61272×10^{19}
	1055.06	107.586	2.93072×10^{-4}	252.042	1	778.172	6.58515×10^{21}
	1.35582	0.138255	3.76616×10^{-7}	0.323890	1.28506×10^{-3}	1	8.46233×10^{18}
	1.60218×10^{-19}	1.63377×10^{-20}	4.45050×10^{-26}	3.82743×10^{-20}	1.51857×10^{-22}	1.18171×10^{-19}	1

1 cal= 4.18605J（計量法）

= 4.184J（熱化学）

= 4.1855J（15℃）

= 4.1868J（国際蒸気表）

仕事率　1 PS(仏馬力)

= 75 kgf·m/s

= 735.499W

放射能	Bq	Ci
	1	2.70270×10^{-11}
	3.7×10^{10}	1

吸収線量	Gy	rad
	1	100
	0.01	1

照射線量	C/kg	R
	1	3876
	2.58×10^{-4}	1

線量当量	Sv	rem
	1	100
	0.01	1

(86年12月26日現在)

Measurement of Activation Reaction Rate Distribution on a Mercury Target with a Lead-reflector and Light-water-moderator for High Energy Proton Bombardment using AGS Accelerator